A Novel Framework for Integration of Abstracted Inspection Data and Structural Health Monitoring for Damage Prognosis of Miter Gates

Manuel A. Vega[a], Zhen Hu[b], Travis B. Fillmore[c], Matthew D. Smith[c], and Michael D. Todd[a*]

[a] *Department of Structural Engineering,*
University of California San Diego,
9500 Gilman Dr., La Jolla, California, USA 92093-0085

[b] *Department of Industrial and Manufacturing Systems Engineering,*
University of Michigan-Dearborn,
4901 Evergreen Rd., Dearborn, Michigan, USA 48187

[c] *Coastal and Hydraulics Laboratory, Engineer Research and Development Center,*
US Army Corps of Engineers,
3909 Halls Ferry Rd, Vicksburg, Mississippi, USA 39180

Abstract

Operational condition assessments, using a discrete rating system, are frequently used by field engineers to assess inland navigation assets and components. Challenges such as the occasional inability to perform inspections (such as the case with locks watered in an operational state) and protocol requirements requiring ratings even when they aren't inspected lead to highly abstracted inspection data, which are also very prone to human error and misinterpretations due to inspections protocol. On the other hand, some navigational locks are equipped with structural health monitoring (SHM) systems to continuously perform assessments from data obtained *in situ*. This paper aims to develop a novel hybrid damage prognosis framework for miter gate component of navigational locks, by mitigating effects of human errors on the condition assessment and integrating the highly abstracted inspection data with the SHM. It overcomes two main challenges, namely (1) there is no physical or empirical model available to model the loss-of-contact degradation in the gate, and (2) the mismatches between the inspection data and the SHM system due to data abstraction. A practical case of monitoring loss-of-contact quoin block demonstrates the efficacy of the proposed framework.

Keywords: Miter Gates; Transition Matrix; Human Error; Gap Growth Model; Damage Estimation; Uncertainty

* Corresponding author: University of California San Diego, 9500 Gilman Dr., La Jolla, California, USA 92093-0085, Email: mdtodd@eng.ucsd.edu

30 **Nomenclature**

a_t, $a(t)$	=	gap length at time t
a_e	=	gap failure threshold
$a(i, j+k)$, $a_{i,\,j+k}$	=	i-th realization of the gap length at the $(j+k)$-th time step
$\mathbf{a}_s(\boldsymbol{\theta}, \mathbf{e})$	=	Samples/realizations obtained of the gap length degradation model parametrized by $\boldsymbol{\theta}$ and $\mathbf{e}$
$\mathbf{e}$	=	vector of estimated parameters, e_i,of mapping function, $h_s(a(t))$
$f_{\mathbf{e}}(\mathbf{e} \mid \boldsymbol{\theta})$	=	joint PDF of e_i given $\boldsymbol{\theta}$
$g(t, \boldsymbol{\theta})$	=	degradation model of the miter gate damage gap at time t given $\boldsymbol{\theta}$
$\hat{g}(a_{k+1}, \mathbf{x}_{k+1})$	=	FE model or surrogate model as a function of a_{k+1} and $\mathbf{x}_{k+1}$
$g_{opt}(\boldsymbol{\theta}; \boldsymbol{\beta}, \mathbf{R})$	=	cost/error function to tune degradation model given $\boldsymbol{\theta}$, $\boldsymbol{\beta}$,and $\mathbf{R}$
$h_{\mathrm{OCA}}(a_t, \boldsymbol{\beta})$	=	protocol mapping function given $\boldsymbol{\beta}$ to map gap length at time t to OCA ratings
$h_s(a(t))$	=	estimated mapping function to map gap length at time t to OCA ratings
$I_{j,t+1}$	=	inspected state I_j (e.g. *A, B, C, D, F* or *CF)* at time $t+1$
I_{t+1}^{tr}	=	underlying true OCA rating at time $t+1$
I_{t+1}^{obs}	=	reported OCA rating from field engineers at time $t+1$
$I_{j,t+1}^{s}$	=	inspected state I_j (e.g. *A, B, C, D, F* or *CF)* at time $t+1$ obtained from degradation model
n_{MCS}	=	number of samples of stochastic degradation model at each time step
N_d	=	distinct degradation stages
N_{PF}	=	number of samples used in the state estimation
N_S	=	number of strain sensors providing data

N_t	=	total number of simulation time steps for stochastic degradation model
$\mathbf{P}$	=	rating transition matrix
$\mathbf{P}_{\text{human}}$	=	human observation error matrix
$\mathbf{P}_{\text{OCA}}$	=	true OCA transition matrix
$\mathbf{P}_{\text{Report}}$	=	reported OCA transition matrix
$\hat{\mathbf{P}}(\boldsymbol{\theta})$	=	simulated transition probabilities of the OCA ratings from the degradation model simulation for given $\boldsymbol{\theta}$
P_{ik}^{h}	=	probability that the reported OCA rating is *k* given that the true OCA rating is *i*
P_{ij}^{OCA}	=	probability of transitioning from true OCA rating *i* at time *t* to true OCA rating *j* at $t+1$
P_{kq}^{R}	=	probability of transitioning from reported OCA rating *k* at time *t* to reported OCA rating *q* at $t+1$
$\Pr\{\cdot\}$	=	probability operator
q_v	=	time-invariant parameter that controls the rate of cooling
Q	=	degradation model parameter to be estimated
Q_i	=	degradation model parameter at degradation stage *i* to be estimated
R	=	OCA rating obtained from continuous monitoring
$\mathbf{s}_i$	=	set of strain measurement data at time step t_i
$\mathbf{s}_{1:k}$	=	set of strain measurement data collected up to t_k
s_{iN_S}	=	strain measurement data at time step t_i at the N_S location
t_l, t_u	=	lower and upper bounds of the time duration of interest (e.g. 1 year)
t_m	=	time when damage threshold is reached
$T_{q_v}(t)$	=	artificial temperature (a time-varying global parameter)
T_{RUL}	=	remaining useful life
$U(t)$	=	stationary standard Gaussian process

w	=	degradation model parameter to be estimated
w_i	=	degradation model parameter at degradation stage *i* to be estimated
$\mathbf{x}_{k+1}$	=	other FE model inputs such water levels and temperature in miter gates
$X(t)$	=	stationary lognormal stochastic process
$\boldsymbol{\beta}$	=	vector of parameters of protocol mapping function
$\Delta\boldsymbol{\theta}(t)$	=	a trial jump distance of the variable $\boldsymbol{\theta}(t)$
ε	=	measurement noise
ζ_x	=	parameter that controls the correlation of $X(t)$ over time
$\boldsymbol{\theta}$	=	vector of model parameters of degradation
$\boldsymbol{\theta}_j$, $\boldsymbol{\theta}(t)$	=	vector of model parameters of degradation stage *j* (or at time *t*)
$\Lambda(E)$	=	indicator function such $\Lambda(E)=1$ if event E is true and $\Lambda(E)=0$ if event E is false
μ_i	=	mean of Gaussian random variable, e_i
σ_e	=	standard deviation of e_i uncorrelated measurement noise, ε
σ_i	=	standard deviation variable of degradation stage *i*
σ_{obs}	=	standard deviation of
σ_x	=	standard deviation of $X(t)$
$\phi(\cdot)$	=	PDF of the standard normal distribution

1 Introduction

Miter gates are common hydraulic steel structures that facilitate passage of boats and watercraft through inland navigation systems as shown in Figure 1. In the United States, the U.S. Army Corps of Engineers (USACE) maintains and operates 236 locks at 191 sites [1]. A closure of a lock due to maintenance or repairs can cost up to $3 million per day to the US economy [2]. This is underscored by the fact that more than half of these structural assets, including miter gates, have surpassed their 50-year economic design life [3]. To help prioritize maintenance and repairs, operational condition assessment (OCA) ratings are performed by USACE inspectors via visual inspections [4]. However, the OCA ratings are highly abstracted and are assigned at a varying frequency, which varies from every year to occurring to a maximum of every 5 years [5]. Recently, several miter gates were equipped with SHM systems that collect strain measurement data in real time [6]. These continuous monitoring systems aim to provide insight regarding deteriorating gates. However, a framework that integrates visual inspections and SHM for damage diagnosis and prognosis has not been developed yet.

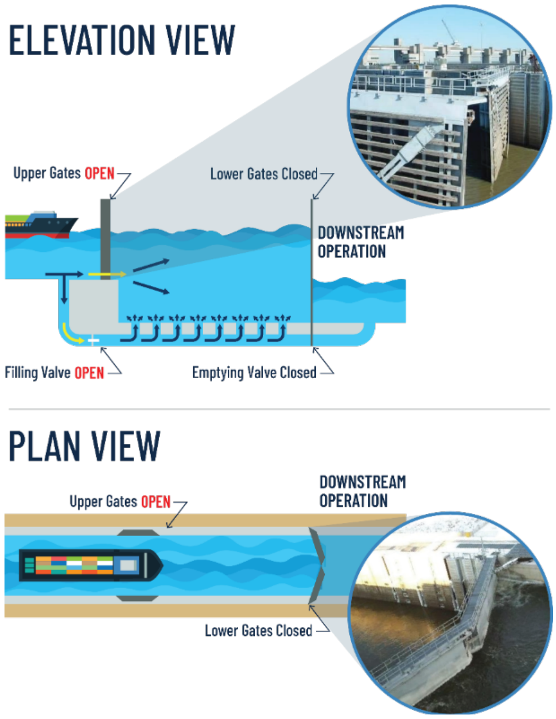

Figure 1: Navigation along miter gates

This paper first gives an overview of the type of damage present in some components of miter gates and how these components are condition-rated based on the field OCA ratings. Section 3 briefly reviews current approaches for failure prognostics of miter gates through the integration of OCA transition matrix with continuous structural health monitoring and proposes a new approach for damage diagnosis and prognosis via a new degradation model derived by mapping the abstracted inspection data into a multistage discrete-time degradation model. The damage diagnosis and prognosis consider the human errors of field engineers in the inspection data. The integration of the derived degradation model with physics-based finite element (FE) model updating will also be studied to perform online damage diagnostics and estimation of the miter gate's remaining useful life. Finally, Section 4 summarizes the important findings of this work and suggest further steps to be taken.

Even though this paper considers a specific application in miter gate damage assessment and prognosis, the developed framework is quite generic; it is easily adaptable to other structural monitoring applications that involve abstracted condition rating data (e.g., like the OCA) and online health monitoring system, such as other miter gate failure modes (e.g., corrosion or pre-tension loss) or other structures including bridges [7–9], pavements [10,11], offshore structures [12], and others [13].

The contributions of this paper are summarized as: (1) it addresses bias in the OCA ratings in the state-transition matrix caused by human observation errors; (2) it maps the abstracted rating state-transition matrix to a failure evolution model; (3) it demonstrates a failure diagnostics and prognostics procedure using structural health monitoring systems based on the failure evolution model; and (4) it demonstrates the developed framework on the very practical case of monitoring loss-of-contact quoin block damage (resulting in "gaps" between the gate and support wall).

In summary, this paper proposes a novel hybrid approach for condition-based maintenance where abstracted OCA ratings subjected to human reporting errors are used to derive a degradation model. Simultaneously, a SHM system is used for damage diagnostics and prognostics based on the derived degradation model. The proposed approach overcomes the challenges that there is no viable degradation model available and there is substantial heterogeneity (i.e., physics-based simulation data, OCA rating data, errors in the OCA rating data, and strain measurement data) in the sources used to inform damage prognostics of miter gate components. Note that, the role of prognosis includes predictions of the future state that inform reliability estimates of the system [14–16]. Predictive capabilities allow informed life cycle management, which target to optimize a certain system performance criterion [17] (e.g. cost, availability, reliability, etc.). Moreover, prognosis capabilities enable engineers to turn available data into information that enhance the current knowledge of the system and also provides a policy to maintain the system optimally.

2 Problem Statement

As mentioned above, there are significant economic implications caused by navigation lock closure, and how to prioritize repairs or other maintenance actions for miter gate components is paramount to minimizing the consequence costs. To understand the prioritization process, there is a need to estimate the extent of damage (i.e., damage diagnosis), and to predict the evolution of damage into the future (i.e., damage prognosis). Any prognosis action fundamentally requires a degradation model of some kind. Ideally, this model would be built from existing time series data or by data generated using a physics-based knowledge of the degradation/failure process. However, in many real-world applications such as with this miter gate case, the lack of existing time series data correlated to deteriorating components and the lack of understanding of the physics behind the damage mechanism evolution impose additional challenges to performing damage prognosis.

As mentioned, OCA ratings are a primary tool used to inform the structural condition state. An OCA rating is a categorical rating given by an inspector, who bases the evaluation on a rating system developed by the USACE Asset Management team, which involves engineering knowledge and information of pre-existing inspections. This rating system classifies structural and non-structural components as A (Excellent), B (Good), C (Fair), D (Poor), F (Failing) and CF (Completely Failed). More detailed definitions can be found in [3]. These ratings are given at the component level of the structural asset (e.g., the miter gate quoin blocks in this paper).

These discrete ratings are highly abstracted, assigned at varying time intervals, and are very prone to human error and to misinterpretations due to inspections protocol [16]. However, these ratings can provide information regarding transitions between different damage rating categories, which may be used to build a degradation model parametrized according to the deterioration of the OCA inspection ratings. In this application, the deterioration of a quoin block component in a miter gate ("damage") is manifested as a "gap" that results in loss of contact beyond the "regular gap" tolerance (~1/32 in.) between the quoin block attached to the gate and the quoin block attached to the wall that supports the gate laterally. The "regular gap" tolerance allows a miter gate to operate and closes when the gate is subjected to hydrostatic loading. The formation of an undesirable "damage gap" beyond the tolerance controls the lateral boundary condition of a miter gate, and significant changes can lead to higher strain/stress in critical components (e.g., the pintle) of the gate. The "gap" or "damage gap" in the subsequent sections of this paper is thus the target damage mechanism considered in this work. More details regarding the different miter gates components mentioned (e.g. quoin blocks, pintle, etc.) can be found here [2].

From historical inspections, a database of the OCA ratings for quoin blocks and other components is available for the past several years, which provides information of the gap transition over the year at the abstracted OCA rating level. Even though the OCA ratings are very prone to human errors, they are the only available data source that contains some form of degradation information of the gate at present. The problem that needs to be solved is how to utilize the abstracted information to effectively perform failure prognostics. In this paper, these reported ratings would be used to build a transition matrix. This reported transition matrix would be combined with a human error matrix to improve the prognosis capabilities of the damage mechanism. This human error matrix will quantify the ability of the inspector to perform correct assessments and false positives/negatives assessments. Diagnosis and prognosis using data-driven models built from solely inspection data (i.e. OCA ratings), however, may lead to large uncertainty in the failure prognosis as shown in previous studies [16,18] and in the case study section.

Beyond these condition ratings, however, structural health monitoring (SHM) systems have been developed for the miter gates to measure their distributed point strain response during operation, providing continuous data streams which may be mined for damage-related information. The SHM measurement systems are coupled with validated high-fidelity physics-based finite element (FE) models [16,19–22], allowing for inference/estimation of the damage gap using the strain measurements. This approach provides more confident estimates of the damage gap state over time. While it is true that the SHM system increases gap inference capabilities, it cannot be used directly to predict the gap degradation over time, since the physics of the gap degradation is complex and not fully understood; SHM alone is not enough to inform decisions regarding prioritizing preventive maintenance.

As described above, however, the historical OCA ratings nevertheless do contain information that may be used to understand the gap degradation over time, even though it is highly abstracted and may be contaminated by human observation errors or bias. Synthesizing, rather than separating, OCA rating transition information and SHM system information has the potential to improve an integrated state awareness (damage state) and state prediction (future damage state).

The two lines of enquiry that are addressed in this paper, therefore, may be summarized as follows:

(1) How should the highly abstracted OCA rating transition information be connected with a high-fidelity FE model for useful integrated damage diagnosis and prognosis?

(2) How should the effects of errors in the OCA rating transition information be mitigated for the damage diagnosis and prognosis?

3 Proposed Method

In this section, a brief review of current methods for failure prognosis of miter gates is summarized. After that, the proposed method is explained in detail.

3.1 Overview

Figure 2 shows the state (damage) variable hierarchy for bearing gaps in a quoin block. This figure shows a hierarchy pyramid that contain three different ways that the gap can be described. The most basic one would use a binary system that would define the state as damaged or undamaged, as time evolves. The next one would be based on discrete state-transition system such as the OCA ratings. For the two ways mentioned, the determination of these deterioration or damage labels would be based on an asset management protocol.

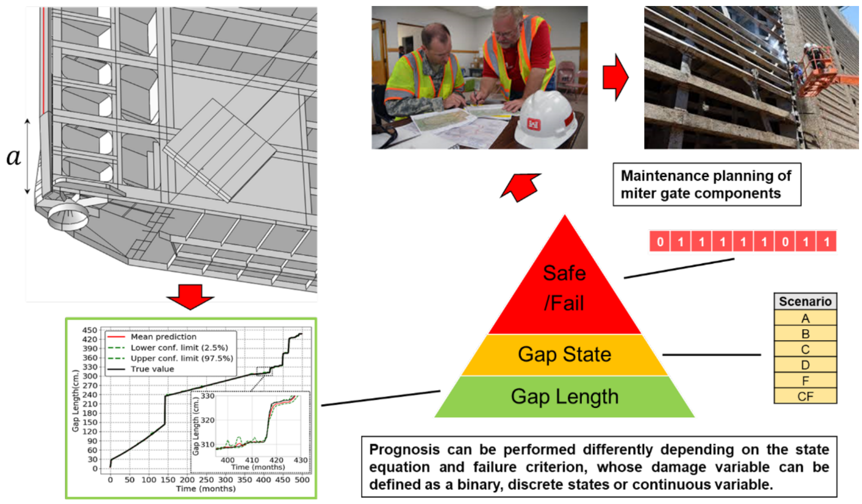

Figure 2: State (damage) variable hierarchy for bearing gap in quoin block

Based on a large historical OCA database, the number of times that a component transitioned from one rating category to another (as determined by engineering expert elicitation) over a given inspection time step can be determined to generate the rating transition matrix [23]. The transition matrix **P** (see Eq. (1)) is defined as a square matrix with nonnegative values that represents how some process "transitions" from one state to the next. In this application, an inspected state at time t, $I_{i,t}$, (with $i = 1\ldots6$, corresponding to the 6 letter ratings specified above), will transition to inspected state at time $t+1$, $I_{j,t+1}$, $j = 1\ldots6$, according to

$$\mathbf{P} = P\left(I_{j,t+1} \middle| I_{i,t}\right) = \begin{bmatrix} P\left(I_{1,t+1} = A \middle| I_{1,t} = A\right) & \cdots & P\left(I_{6,t+1} = CF \middle| I_{1,t} = A\right) \\ \vdots & \ddots & \vdots \\ P\left(I_{1,t+1} = A \middle| I_{6,t} = CF\right) & \cdots & P\left(I_{6,t+1} = CF \middle| I_{6,t} = CF\right) \end{bmatrix}. \quad (1)$$

In Eq. (1), only the upper triangular components were considered to simulate component deterioration; the lower triangular components would represent improvements or repairs (transitions from a worse condition to a better condition), and for the purposes of this analysis, they were ignored. Further details on this transition matrix can be found in [16,24,25].

Furthermore, the bearing gaps may also be modelled at the continuous level (i.e. gap-length level at the bottom of the pyramid) based on continuous structural health monitoring (SHM) systems. In order to address the above-mentioned *first line of enquiry*, which is to connect the highly abstracted OCA rating transition information with a high-fidelity FE model for useful integrated damage diagnosis and prognosis, Vega et al. [16] developed a hybrid prognostic approach by converting the continuous level into gap-state level as illustrated in Fig. 3. Even though the approach developed in [16] allows for the integration of SHM with Markov analysis for integrated damage diagnosis and prognosis, the component degradation modeling at the discrete state-transition level could lead to wide uncertainty in the prognostics even when using recursive model updating.

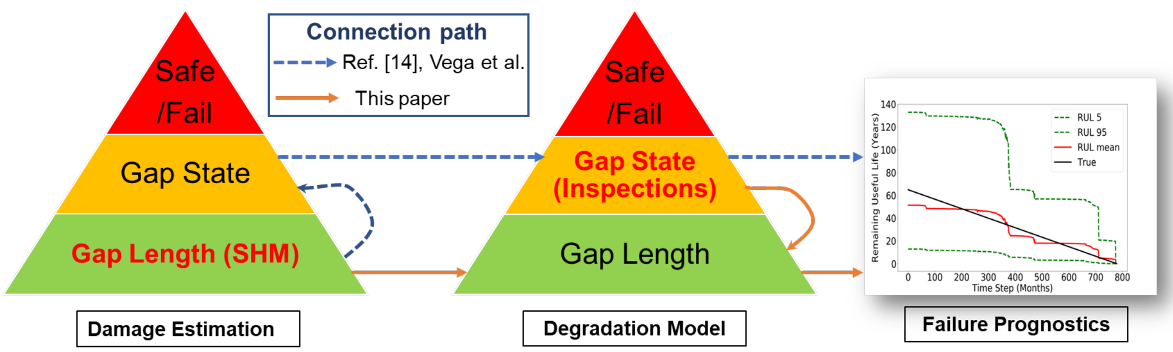

Figure 3: Comparison of the connection paths between damage estimation and degradation model for the methods presented in Vega et al. [16] and this paper

In this paper, as illustrated in Fig. 3, instead of converting the damage estimation at gap-length level into abstracted gap-state level for prognostics, the degradation model is built at the continuous gap-length level by tuning the degradation model parameters to agree with the Markov transition matrix built from the OCA ratings (gap-state level). After that, failure prognostics at the gap-length level is performed. The goal is to meaningfully increase the confidence in the miter gate failure prognostics beyond on what is was proposed in [16] to achieve an effective and useful decision-making capability. In addition to the tuning of degradation model parameters using data at gap-state level, a new approach will also be developed to address the errors in the OCA transition matrix due to human observation variability, thereby addressing the *second line of enquiry* mentioned above).

Let $a_t = g(t, \boldsymbol{\theta})$ be the underlying degradation model of the miter gate damage gap, where a_t is the gap length at time *t*, and $\boldsymbol{\theta}$ is a vector of model parameters. Fig. 4 shows the relationship among the degradation model, OCA ratings, and the reported OCA ratings by the field engineers. As shown in Fig. 4, the OCA protocol maps the gap length, a_t, (i.e., the output of the unknown degradation model) into OCA ratings as if the protocol were strictly and accurately followed by the field engineers. Due to human observation error and variability, however, the OCA ratings reported by the field engineers as indicated in Fig. 4 may not be the same as the "true" rating that better represents the condition; this is proven true for inspectors in many application domains [26].

One of the objectives of the proposed method is to infer the unknown degradation model, $a_t = g(t, \boldsymbol{\theta})$, using *the reported OCA ratings*, which include the human variability or errors in the rating reporting process. The inferred degradation model will then be used for *integrated* damage diagnostics and prognostics of the miter gate. As shown in Fig. 4, the inference of the unknown degradation model in the proposed framework is accomplished through two steps:

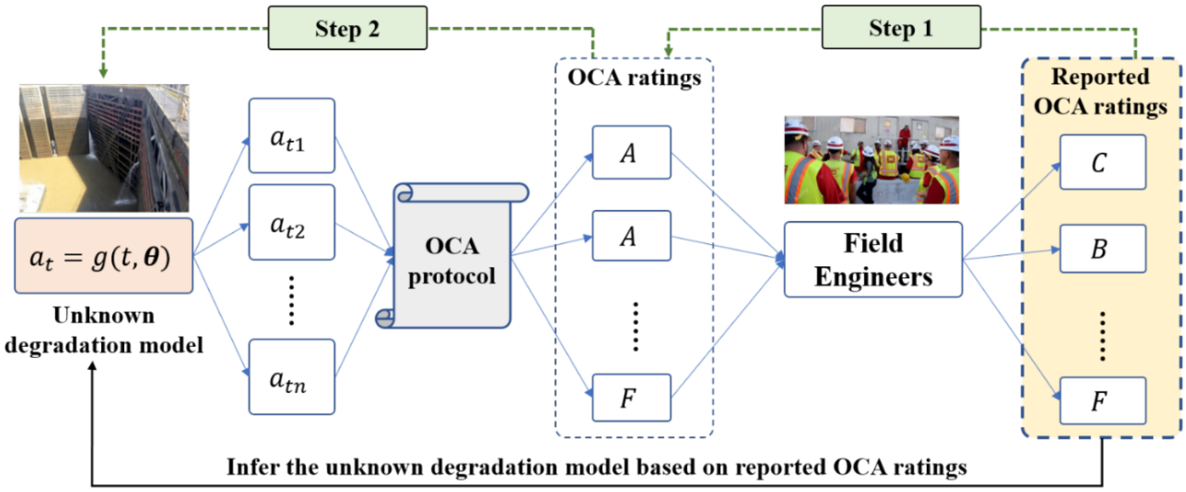

Figure 4: Relationship among the gap degradation, OCA ratings, and the reported OCA ratings

- **Step 1**: Mapping of the reported OCA ratings to the underlying condition for a given OCA protocol, by considering the human observation errors of field engineers in reporting.
- **Step 2**: Estimation of the degradation model parameters ($\boldsymbol{\theta}$) based on the obtained true OCA ratings (i.e. true OCA transition matrix).

In the next section, these two steps will be explained in detail.

3.2 Mapping of the reported OCA rating transition matrix to the true transition matrix

In order to map the reported OCA rating transition matrix to the underlying "true" OCA transition matrix, the underlying true OCA rating is defined at time *t* as I_t^{tr} and that at *t*+1 as I_{t+1}^{tr}, the reported OCA rating from field engineers at time *t* as I_t^{obs} and that at time *t*+1 as I_{t+1}^{obs}. Based on these definitions, the true OCA transition matrix $\mathbf{P}_{\text{OCA}}$ (i.e. OCA "ideal" protocol is strictly followed) is denoted as

$$\mathbf{P}_{\mathrm{OCA}} = \begin{bmatrix} P_{11}^{OCA} & P_{12}^{OCA} & \cdots & P_{16}^{OCA} \\ 0 & P_{22}^{OCA} & \cdots & P_{26}^{OCA} \\ \vdots & \vdots & \ddots & \vdots \\ 0 & 0 & \cdots & P_{66}^{OCA} \end{bmatrix}, \tag{2}$$

where $P_{ij}^{OCA} = \Pr\{I_{t+1}^{tr} = j \mid I_t^{tr} = i\} \triangleq P(I_{j,t+1}^{tr} \big| I_{i,t}^{tr}), \forall i = 1, 2, \cdots, 6; j = i, \cdots, 6$ represents the probability of transitioning from true OCA rating i at time t to true OCA rating j at t+1.

Similarly, the reported transition matrix, built from the OCA ratings reported by field engineers, is denoted as

$$\mathbf{P}_{\mathrm{Report}} = \begin{bmatrix} P_{11}^{R} & P_{12}^{R} & \cdots & P_{16}^{R} \\ 0 & P_{22}^{R} & \cdots & P_{26}^{R} \\ \vdots & \vdots & \ddots & \vdots \\ 0 & 0 & \cdots & P_{66}^{R} \end{bmatrix}, \tag{3}$$

where $P_{kq}^{R} = \Pr\{I_{t+1}^{obs} = q \mid I_t^{obs} = k\}, \forall k = 1, 2, \cdots, 6; q = k, \cdots, 6$ is the probability of transitioning from reported OCA rating k at time t to reported OCA rating q at t+1, based on the reported OCA ratings. In addition, from the reported OCA ratings the state probabilities $\Pr\{I_t^{obs} = k\}, k = 1, 2, \cdots, 6$ and $\Pr\{I_{t+1}^{obs} = q\}, q = 1, 2, \cdots, 6$ may also be obtained.

The goal of Step 1 of the proposed method (see Fig. 4) is to map $\mathbf{P}_{\mathrm{Report}}$ to $\mathbf{P}_{\mathrm{OCA}}$. To achieve this goal, the human observation error matrix is defined as

$$\mathbf{P}_{\mathrm{human}} = \begin{bmatrix} P_{11}^{h} & P_{12}^{h} & \cdots & P_{16}^{h} \\ 0 & P_{22}^{h} & \cdots & P_{26}^{h} \\ \vdots & \vdots & \ddots & \vdots \\ 0 & 0 & \cdots & P_{66}^{h} \end{bmatrix}, \tag{4}$$

in which $P_{ik}^{h} = \Pr\{I_t^{obs} = k \mid I_t^{tr} = i\}$ is the probability that the reported OCA rating is k given that the true OCA rating is i.

Based on the above definitions of $\mathbf{P}_{\text{OCA}}$, $\mathbf{P}_{\text{Report}}$, and $\mathbf{P}_{\text{human}}$, the reported and true OCA ratings are connected using a Bayesian network as shown in Fig. 5.

From the above Bayesian network, the following conditional probability tables (CPTs) are obtained:

$$\begin{aligned}&\Pr\{I_t^{obs}=k \mid I_t^{tr}=i\}=P_{ik}^{h}, \forall i=1,2,\cdots,6; k=1,2,\cdots,6;\\&\Pr\{I_{t+1}^{obs}=q \mid I_{t+1}^{tr}=j\}=P_{jq}^{h}, \forall j=1,2,\cdots,6; q=1,2,\cdots,6;\end{aligned} \tag{5}$$

and

$$\begin{aligned}&\Pr\{I_{t+1}^{obs}=q \mid (I_{t+1}^{tr}=j, I_t^{obs}=k)\}\\&=\frac{\Pr\{I_{t+1}^{obs}=q, I_{t+1}^{tr}=j, I_t^{obs}=k\}}{\Pr\{I_{t+1}^{tr}=j, I_t^{obs}=k\}},\\&=\frac{\Pr\{I_t^{obs}=k \mid I_{t+1}^{obs}=q, I_{t+1}^{tr}=j\}\Pr\{I_{t+1}^{obs}=q \mid I_{t+1}^{tr}=j\}\Pr\{I_{t+1}^{tr}=j\}}{\Pr\{I_{t+1}^{tr}=j, I_t^{obs}=k\}}.\end{aligned} \tag{6}$$

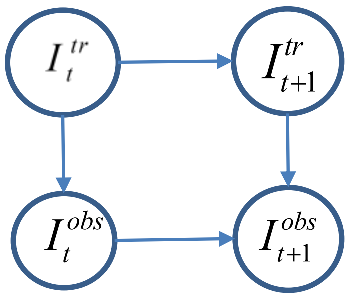

Figure 5: A Bayesian network connecting the observed and the true OCA ratings

Since the lower triangular components of $\mathbf{P}_{\text{Report}}$ are all zero, the following marginal probability is written

$$\Pr\{I_{t+1}^{tr}=j, I_t^{obs}=k\}=\sum_{w=k}^{6}\Pr\{I_{t+1}^{obs}=w, I_{t+1}^{tr}=j, I_t^{obs}=k\}. \tag{7}$$

With the above CPTs, the task is to obtain the true OCA transition matrix by solving $\Pr\{I_{t+1}^{tr}=j \mid I_t^{tr}=i\}, \forall i=1,2,\cdots,6; j=i,\cdots,6$ in the Bayesian network shown in Fig. 5. Using $\Pr\{I_{t+1}^{obs}=q\}, q=1,2,\cdots,6$, the following marginal probability is written

$$\begin{aligned}\Pr\{I_{t+1}^{obs}=q\} &= \sum_{j=1}^{6}\Pr\{I_{t+1}^{obs}=q,\, I_{t+1}^{tr}=j\}, \forall q=1,2,\cdots,6;\\ &= \sum_{j=1}^{6}\Pr\{I_{t+1}^{obs}=q \mid I_{t+1}^{tr}=j\}\Pr\{I_{t+1}^{tr}=j\}, \forall q=1,2,\cdots,6,\end{aligned} \tag{8}$$

which may be elucidated more clearly in matrix form as

$$\begin{bmatrix}\Pr\{I_{t+1}^{obs}=1\}\\ \Pr\{I_{t+1}^{obs}=2\}\\ \vdots\\ \Pr\{I_{t+1}^{obs}=2\}\end{bmatrix}=\begin{bmatrix}P_{11}^{h} & P_{12}^{h} & \cdots & P_{16}^{h}\\ P_{21}^{h} & P_{22}^{h} & \cdots & P_{26}^{h}\\ \vdots & \vdots & \ddots & \vdots\\ P_{61}^{h} & P_{62}^{h} & \cdots & P_{66}^{h}\end{bmatrix}\begin{bmatrix}\Pr\{I_{t+1}^{tr}=1\}\\ \Pr\{I_{t+1}^{tr}=2\}\\ \vdots\\ \Pr\{I_{t+1}^{tr}=6\}\end{bmatrix}. \tag{9}$$

Based on Eq. (9), $\Pr\{I_{t+1}^{tr}=j\}, \forall j=1,2,\cdots,6$ may be solved using $\mathbf{P}_{\text{human}}$ and $\Pr\{I_{t+1}^{obs}=q\}, q=1,2,\cdots,6$. In this paper, a constrained least-squares method is used to solve Eq. (9) to ensure that the obtained probability estimates are in the range of [0, 1]. In order to estimate $\Pr\{I_{t+1}^{tr}=j \mid I_{t}^{tr}=i\}, \forall i=1,2,\cdots,6; j=i,\cdots,6$, a derivation of the term $\Pr\{I_{t}^{obs}=k, I_{t+1}^{obs}=q\}=P_{kq}^{R}\Pr\{I_{t}^{obs}=k\}$ is performed (see **Appendix A** for derivations) as follows:

$$\begin{aligned}&P_{kq}^{R}\Pr\{I_{t}^{obs}=k\}\\ &=\sum_{i=1}^{6}\sum_{j=i}^{6}\left(\frac{\Pr\{I_{t}^{obs}=k \mid I_{t+1}^{obs}=q, I_{t+1}^{tr}=j\}P_{jq}^{h}\Pr\{I_{t+1}^{tr}=j\}}{\sum_{w=k}^{6}\Pr\{I_{t}^{obs}=k \mid I_{t+1}^{obs}=w, I_{t+1}^{tr}=j\}P_{jw}^{h}\Pr\{I_{t+1}^{tr}=j\}}P_{ik}^{h}\right)\Pr\{I_{t+1}^{tr}=j, I_{t}^{tr}=i\}.\end{aligned} \tag{10}$$

In order to make $\Pr\{I_{t+1}^{tr}=j \mid I_{t}^{tr}=i\}, \forall i=1,2,\cdots,6; j=i,\cdots,6$ solvable given the current available information ($\mathbf{P}_{\text{Report}}$ and $\mathbf{P}_{\text{human}}$), a conditional independence is assumed, given by $\Pr\{I_{t}^{obs}=k \mid I_{t+1}^{obs}=q, I_{t+1}^{tr}=j\}=\Pr\{I_{t}^{obs}=k \mid I_{t+1}^{obs}=q\}$. This is a reasonable assumption for the Bayesian network structure given in Fig. 5, since the resulting joint probability mass function $\Pr\{I_{t+1}^{obs}=q, I_{t+1}^{tr}=j, I_{t}^{obs}=k\}$ satisfies the constraints of all the current given information in

$\mathbf{P}_{\text{Report}}$ and $\mathbf{P}_{\text{human}}$. Based on this assumption, the conditional probability and Bayes rule are exploited

$$\begin{aligned}&\Pr\{I_{t+1}^{obs}=q, I_{t+1}^{tr}=j, I_{t}^{obs}=k\}\\&=\Pr\{I_{t}^{obs}=k \mid I_{t+1}^{obs}=q\}P_{jq}^{h}\Pr\{I_{t+1}^{tr}=j\}=\frac{P_{kq}^{R}\Pr\{I_{t}^{obs}=k\}P_{jq}^{h}\Pr\{I_{t+1}^{tr}=j\}}{\Pr\{I_{t+1}^{obs}=q\}}, \forall q\geq k.\end{aligned} \tag{11}$$

Substituting Eq. (11) into Eq. (10) as follows

$$\begin{aligned}&P_{kq}^{R}\Pr\{I_{t}^{obs}=k\}\\&=\sum_{i=1}^{6}\sum_{j=i}^{6}\left(\frac{\dfrac{P_{kq}^{R}\Pr\{I_{t}^{obs}=k\}P_{jq}^{h}\Pr\{I_{t+1}^{tr}=j\}}{\Pr\{I_{t+1}^{obs}=q\}}}{\sum_{w=k}^{6}\left(\dfrac{P_{kw}^{R}\Pr\{I_{t}^{obs}=k\}P_{jw}^{h}\Pr\{I_{t+1}^{tr}=j\}}{\Pr\{I_{t+1}^{obs}=w\}}\right)}P_{ik}^{h}\right)\Pr\{I_{t+1}^{tr}=j, I_{t}^{tr}=i\}.\end{aligned} \tag{12}$$

Defining $P_{ijkq}\triangleq\dfrac{\dfrac{P_{kq}^{R}\Pr\{I_{t}^{obs}=k\}P_{jq}^{h}\Pr\{I_{t+1}^{tr}=j\}}{\Pr\{I_{t+1}^{obs}=q\}}}{\sum_{w=k}^{6}\left(\dfrac{P_{kw}^{R}\Pr\{I_{t}^{obs}=k\}P_{jw}^{h}\Pr\{I_{t+1}^{tr}=j\}}{\Pr\{I_{t+1}^{obs}=w\}}\right)}P_{ik}^{h}$, it follows that

$$P_{kq}^{R}\Pr\{I_{t}^{obs}=k\}=\sum_{i,j=1}^{6}P_{ijkq}\Pr\{I_{t+1}^{tr}=j, I_{t}^{tr}=i\} \tag{13}$$

which again elucidated in matrix form is

$$\begin{bmatrix}P_{J,1}\\P_{J,2}\\\vdots\\P_{J,20}\\P_{J,21}\end{bmatrix}_{21\times1}=\begin{bmatrix}P_{J,1,1}^{h} & P_{J,1,2}^{h} & \cdots & P_{J,1,20}^{h} & P_{J,1,21}^{h}\\P_{J,2,1}^{h} & P_{J,2,2}^{h} & \cdots & P_{J,2,20}^{h} & P_{J,2,21}^{h}\\\vdots & \vdots & \ddots & \vdots & \vdots\\P_{J,20,1}^{h} & P_{J,20,2}^{h} & \cdots & P_{J,20,20}^{h} & P_{J,20,21}^{h}\\P_{J,21,1}^{h} & P_{J,21,2}^{h} & \cdots & P_{J,21,20}^{h} & P_{J,21,21}^{h}\end{bmatrix}_{21\times21}\begin{bmatrix}P_{J,1}^{OCA}\\P_{J,2}^{OCA}\\\vdots\\P_{J,20}^{OCA}\\P_{J,21}^{OCA}\end{bmatrix}_{21\times1}, \tag{14}$$

where $P_{J,x}=P_{kq}^{R}\Pr\{I_{t}^{obs}=k\}$, $P_{J,y}^{OCA}=\Pr\{I_{t+1}^{tr}=j, I_{t}^{tr}=i\}$, $P_{J,x,y}^{h}=P_{ijkq}$, and the indices are related to each other by

$$x = \begin{cases} q, \text{ if } k = 1 \\ (q-k+1) + \sum_{s=1}^{k-1}(6-s+1), \text{ otherwise} \end{cases}, \forall q \geq k, \quad (15)$$

and

$$y = \begin{cases} j, \text{ if } i = 1 \\ (j-i+1) + \sum_{s=1}^{i-1}(6-s+1), \text{ otherwise} \end{cases}, \forall j \geq i. \quad (16)$$

Using Eq. (14), $P_{J,y}^{OCA} = \Pr\{I_{t+1}^{tr} = j, I_t^{tr} = i\}, \forall i = 1, 2, \cdots, 6; j = i, \cdots, 6$ may be solved similarly as in Eq. (9) using the constrained least-squares method. Using the above equations (Eq. (5) through (16)), the reported OCA rating transition matrix $\mathbf{P}_{\text{Report}}$ is mapped into the underlying true OCA rating transition matrix $\mathbf{P}_{\text{OCA}}$ considering the human observation errors $\mathbf{P}_{\text{human}}$.

As shown above, the estimation of the $\mathbf{P}_{\text{OCA}}$ matrix depends on the $\mathbf{P}_{\text{human}}$ matrix, which is assumed to be known in this work. However, when it is unknown, there are two approaches to estimate the $\mathbf{P}_{\text{human}}$ matrix. One way is to do a benchmark study using a statistically significant set of data focused on visual OCA ratings, similar to [26]. This consists on bringing inspectors to asses miter gate component with previously known damage condition to estimate $P_{ik}^{h} = \Pr\{I_t^{obs} = k \mid I_t^{tr} = i\}$. The other approach is to make the best possible estimation of $\mathbf{P}_{\text{human}}$, using previously collected data to inform a prior distribution for the parameters of the degradation model (described in the next section, which can be later updated using the continous SHM data). This second approach, when used in conjunction with Bayesian methods, is more desirable since it enables the continous updating of the degradation model for a specific case/structure using SHM data. Further work that is beyond the scope of this paper would be required to fully address any of these mentioned approaches. The next section will discuss how to estimate the degradation model parameters $\boldsymbol{\theta}$ of $a_t = g(t, \boldsymbol{\theta})$ using the transition matrix $\mathbf{P}_{\text{OCA}}$.

3.3 Estimation of the degradation model parameters

As noted in Step 2 in Fig. 4, in order to establish a connection between the degradation model $a_t = g(t, \boldsymbol{\theta})$ and the OCA transition matrix $\mathbf{P}_{\text{OCA}}$, a mapping function is defined for the OCA protocol as below

$$R = h_{\text{OCA}}(a_t, \boldsymbol{\beta}) = \begin{cases} I_{1,t} = A, a \in [0, \beta_1] \\ I_{2,t} = B, a_t \in [\beta_1, \beta_2] \\ I_{3,t} = C, a_t \in [\beta_2, \beta_3] \\ I_{4,t} = D, a_t \in [\beta_3, \beta_4] \\ I_{5,t} = F, a_t \in [\beta_4, \beta_5] \\ I_{6,t} = CF, a_t \in [\beta_5, \infty) \end{cases}, \tag{17}$$

where R is the OCA rating, a_t is the gap length, and $\boldsymbol{\beta} = [\beta_1, \beta_2, \beta_3, \beta_4, \beta_5]$ is a vector of parameters of the mapping function related to the OCA protocol.

In the proposed method, the unknown parameters $\boldsymbol{\theta}$ are estimated for given set of parameters $\boldsymbol{\beta}$ that define the mapping function (i.e. Eq. (17)), given the degradation model $a_t = g(t, \boldsymbol{\theta})$ and the true OCA transition matrix, $\mathbf{P}_{\text{OCA}}$, shown in Sec. 3.2. After that, diagnostics and prognostics are performed based on the estimated $\boldsymbol{\theta}$.

The task of estimating $\boldsymbol{\theta}$ relies on solving the following optimization problem

$$\begin{aligned} &\boldsymbol{\theta}^* = \arg\min_{\boldsymbol{\theta}} \{g_{opt}(\boldsymbol{\theta}; \boldsymbol{\beta}, \mathbf{P}_{\text{OCA}})\}, \\ &s.t. \boldsymbol{\theta} \in \Omega, \end{aligned} \tag{18}$$

where $g_{opt}(\boldsymbol{\theta}; \boldsymbol{\beta}, \mathbf{P}_{\text{OCA}})$ is a cost function of the optimization model, and Ω is the domain of $\boldsymbol{\theta}$. In the above optimization model, the cost function $g_{opt}(\boldsymbol{\theta}; \boldsymbol{\beta}, \mathbf{P}_{\text{OCA}})$ is defined as

$$g_{opt}(\boldsymbol{\theta};\ \boldsymbol{\beta}, \mathbf{P}_{\text{OCA}}) = \left\|\hat{\mathbf{P}}(\boldsymbol{\theta}) - \mathbf{P}_{\text{OCA}}\right\|_2, \\ = \sum_{i=1}^{6}\sum_{j=i}^{6}(\hat{P}(I^s_{j,t+1} \mid I^s_{i,t}; \boldsymbol{\theta}) - P(I^{tr}_{j,t+1} \mid I^{tr}_{i,t}))^2, \tag{19}$$

in which $I^s_{i,t}$ and $I^s_{j,t+1}$ are the inspected state (e.g. *A, B, C, D, F* or *CF)* at time t and $t+1$ respectively obtained from the degradation simulation and mapping function, $h_{\text{OCA}}(a_t, \boldsymbol{\beta})$. For $P(I^{tr}_{j,t+1} \mid I^{tr}_{i,t}) \triangleq \Pr\{I^{tr}_{t+1} = j \mid I^{tr}_t = i\}$, the reader can refer to the definitions of Eq. (2), $\hat{\mathbf{P}}(\boldsymbol{\theta}) \triangleq \{\hat{P}(I^s_{j,t+1} \mid I^s_{i,t}; \boldsymbol{\theta}), i = 1, 2, \cdots, 6;\ j = i, \cdots, 6\}$ is the simulated transition probabilities of the OCA ratings from the degradation model simulation for given $\boldsymbol{\theta}$, and $\mathbf{P}_{\text{OCA}}$ is the true OCA transition matrix (i.e. Eq. (2)) obtained from Sec. 3.2 based on the reported OCA transition matrix and human observation error matrix.

It should be noted that, theoretically speaking, the optimization model Eq. (19) may also be formulated directly from the reported OCA transition matrix $\mathbf{P}_{\text{Report}}$ perspective by coupling the approach developed in this section with the forward uncertainty propagation of the OCA ratings based on the human error observation matrices. That kind of formulation may be considered as an alternative approach to the proposed method and will be compared in future work. The benefit of using $\mathbf{P}_{\text{OCA}}$ in Eq. (19) is two-fold: first, the identification of $\mathbf{P}_{\text{OCA}}$ in Sec. 3.2 allows to perform failure prognostics with $\mathbf{P}_{\text{OCA}}$ instead of $\mathbf{P}_{\text{Report}}$ using the approach developed in [16]. Using $\mathbf{P}_{\text{OCA}}$ to replace $\mathbf{P}_{\text{Report}}$ in transition matrix-based prognostics will improve the accuracy of failure prognostics since $\mathbf{P}_{\text{OCA}}$ mitigates the effects of human observation errors. Second, the formulation given in Eq. (19) eliminates process of uncertainty propagation step from $\mathbf{P}_{\text{OCA}}$ to $\mathbf{P}_{\text{Report}}$ in estimating $\boldsymbol{\theta}$, which reduces the complexity of the optimization process.

As shown in Eq. (19), the estimation of $\hat{\mathbf{P}}(\boldsymbol{\theta})$ for a given $\boldsymbol{\theta}$ is the key for the optimization-based method to minimize the L2 error norm between the underlying true OCA transition matrix, $\mathbf{P}_{\text{OCA}}$, and the estimated transition matrix $\hat{\mathbf{P}}(\boldsymbol{\theta})$ obtained from the estimated multi-stage continuous degradation model. The next section will discuss in detail on how to estimate $\hat{\mathbf{P}}(\boldsymbol{\theta})$ for a given $\boldsymbol{\theta}$. After that, an explanation will be given of how to solve Eq. (19) based on the estimation of multi-stage continuous degradation model.

3.3.1 Prediction of OCA rating transition matrix $\hat{\mathbf{P}}(\boldsymbol{\theta})$ *for given* $\boldsymbol{\theta}$

(a) Selection of degradation model

As mentioned earlier, there is a need for a degradation model whose OCA transition matrix prediction, $\hat{\mathbf{P}}(\boldsymbol{\theta})$, resembles the true OCA transition matrix, $\mathbf{P}_{\text{OCA}}$. A variation of the stochastic model proposed by Yang and Manning [27], which is referred as the Yang and Manning model and reviewed in **Appendix B**, is used. This model allows flexibility when considering the abstracted OCA data and the lack of the understanding of the physics of the damage evolution of bearing gaps.

To account for the effect of degradation stages over continuous time, the Yang and Manning model (see Appendix B for details) is generalized as below

$$\frac{da(t)}{dt} = \exp(\sigma(t)U(t))Q(t)(a(t))^{w(t)}, \tag{20}$$

where $U(t)$ is a stationary standard Gaussian process with auto-correlation function given by Eq. (51) in Appendix B, $\sigma(t)$, $Q(t)$, and $w(t)$ are parameters determined through gap length $a(t)$ as follows

$$\begin{cases} \sigma(t) = \sigma_j \\ Q(t) = Q_j \text{, where } j = h_s(a(t)), \forall j = 1, \cdots, N_d, \\ w(t) = w_j \end{cases} \tag{21}$$

in which N_d is the number of degradation stages, $j = h_s(a(t))$ is a function that discretely maps gap length $a(t)$ into degradation stages as below

$$j = h_s(a(t)) = \begin{cases} 1, \text{ if } a(t) \in [0, e_1], \\ 2, \text{ if } a(t) \in [e_1, e_2], \\ \vdots \\ N_d, \text{ if } a(t) \in [e_{N_d-1}, \infty), \end{cases} , \tag{22}$$

where $e_i < e_{i+1}, \forall i = 1, 2, \cdots, N_d - 2$ are the threshold gap lengths that determine the transition of degradation stages. Note that the mapping function $j = h_s(a(t)))$ for the gap growth model is different from the mapping function (i.e. $R = h_{OCA}(a_t, \boldsymbol{\beta}))$ defined by the OCA protocol. The mapping function $j = h_s(a(t))$ is governed by the underlying degradation physics, while $R = h_{OCA}(a_t, \boldsymbol{\beta})$ is defined by the engineers using OCA protocols.

Moreover, in order to account for the randomness of the threshold gap lengths that govern the transition of degradation stages, $e_i, \forall i = 1, 2, \cdots, N_d - 1$ are described as Gaussian random variables as follows

$$e_i \sim N(\mu_i, \sigma_e^2), \forall i = 1, 2, \cdots, N_d - 1, \tag{23}$$

with mean μ_i and standard deviation σ_e.

In the discrete time domain, the above degradation model is rewritten as

$$a(t_{k+1}) = a(t_k) + \exp(\sigma(t_{k+1})U(t_{k+1}))Q(t_{k+1})(a(t_k))^{w(t_{k+1})}, \forall k = 1, 2, \cdots, N_t, \tag{24}$$

$$\begin{cases} \sigma(t_{k+1}) = \sigma_j \\ Q(t_{k+1}) = Q_j \\ w(t_{k+1}) = w_j \end{cases}, \text{ where } j = h_s(a(t_k)), \forall j = 1, \cdots, N_d, \tag{25}$$

where N_t is the number of analysis time steps in the time duration of interest.

To summarize, in the selected degradation model, the parameters $\boldsymbol{\theta}$ of the degradation model include the following parameters

$$\boldsymbol{\theta} \triangleq \left\{\boldsymbol{\theta}_1, \boldsymbol{\theta}_2, \cdots, \boldsymbol{\theta}_{N_d}, \zeta, \mu_1, \mu_2, \cdots, \mu_{N_d-1}, \sigma_e\right\}, \tag{26}$$

where $\boldsymbol{\theta}_j \triangleq \{\sigma_j, Q_j, w_j, j = 1, 2, \cdots, N_d\}$.

The next section will discuss the prediction of $\hat{\mathbf{P}}(\boldsymbol{\theta})$ for a given $\boldsymbol{\theta}$.

(b) Prediction of $\hat{\mathbf{P}}(\boldsymbol{\theta})$ using the degradation model

Based on the above degradation model, for given $\boldsymbol{\theta}$ and $\mathbf{e}$, according to the derivations given in **Appendix C**, $\hat{P}(I^s_{j,t+1} \mid I^s_{i,t}; \boldsymbol{\theta}, \mathbf{e})$, $\forall i = 1, 2, \cdots, 6; j = i, \cdots, 6$, are estimated based on the degradation simulation as follows

$$\hat{P}(I^s_{j,t+1} \mid I^s_{i,t}; \boldsymbol{\theta}, \mathbf{e}) \approx \frac{1}{(N_t - 12) n_{MCS}} \sum_{k=1}^{N_t - 12} \frac{\sum_{q=1}^{n_{MCS}} \Lambda((\beta_{i-1} \le a_{q,k} < \beta_i) \cap (\beta_{j-1} \le a_{q,k+12} < \beta_j))}{\sum_{q=1}^{n_{MCS}} \Lambda(\beta_{i-1} \le a_{q,k} < \beta_i)}, \tag{27}$$

where $\Lambda(\cdot)$ is an indicator function defined in Eq. (58) in Appendix C and $a_{q,k}$ is the simulated q-th realization of gap length at time step t_k (see Appendix C for details).

The above probability estimate is conditioned on $\boldsymbol{\theta}$ and $\mathbf{e}$. After considering the uncertainty in threshold gap lengths, $\mathbf{e} = [e_1, e_2, \cdots, e_{N_d-1}]$ that determine the transition of degradation stages, the marginalization of $\hat{P}(I^s_{j,t+1} \mid I^s_{i,t}; \boldsymbol{\theta})$ may be written as

$$\begin{aligned} \hat{P}(I^s_{j,t+1} \mid I^s_{i,t}; \boldsymbol{\theta}) &= \int \hat{P}(I^s_{j,t+1} \mid I^s_{i,t}; \boldsymbol{\theta}, \mathbf{e}) f_{\mathbf{e}}(\mathbf{e} \mid \boldsymbol{\theta}) d\mathbf{e}, \\ &= \int\int \cdots \int \hat{P}(I^s_{j,t+1} \mid I^s_{i,t}; \boldsymbol{\theta}, \mathbf{e}) \prod_{k=1}^{N_d-1} \phi\left(\frac{e_i - \mu_i}{\sigma_e}\right) de_1 de_2 \cdots de_{N_d-1}, \end{aligned} \tag{28}$$

where $f_{\mathbf{e}}(\mathbf{e}\,|\,\boldsymbol{\theta})$ is the joint PDF of e_i, and $e_i < e_{i+1}, \forall i = 1, 2, \cdots, N_d - 2$, and $\phi(\cdot)$ is the PDF of the standard normal distribution.

In this paper, a sampling-based approach is employed to estimate Eq. (28). Using the above equations and derivations in Appendix C, $\hat{\mathbf{P}}(\boldsymbol{\theta}) \triangleq \{\hat{P}(I^s_{j,t+1}\,|\,I^s_{i,t};\boldsymbol{\theta}), i = 1, 2, \cdots, 6; j = i, \cdots, 6\}$ may be estimated for given $\boldsymbol{\theta}$. The estimated $\hat{\mathbf{P}}(\boldsymbol{\theta})$ may then be used in Eq. (19) to obtain the parameters $\boldsymbol{\theta}$ of the degradation model. Table 1 provides a pseudocode for this process.

Table 1: Estimation of $\hat{\mathbf{P}}(\boldsymbol{\theta})$ for given $\boldsymbol{\theta} \triangleq \left\{\boldsymbol{\theta}_1, \boldsymbol{\theta}_2, \cdots, \boldsymbol{\theta}_{N_d}, \zeta, \mu_1, \mu_2, \cdots, \mu_{N_d-1}, \sigma_e\right\}$

Step	Description
1	**Initialization**: Generate samples of $U(t_1), \cdots, U(t_{N_t})$ for a given correlation length ζ, samples of $e_i < e_{i+1}, \forall i = 1, 2, \cdots, N_d - 2$ based on $\mu_1, \mu_2, \cdots, \mu_{N_d-1}, \sigma_e$, and initial samples of $a(t_0)$
2	Sort the samples of $e_i < e_{i+1}, \forall i = 1, 2, \cdots, N_d - 1$
3	**For** $k = 1, 2, \cdots, N_t$:
4	Map gap length $a(t_{k-1})$ into degradation stage using Eq. (22)
5	Obtain samples of $a(t_k)$ using Eqs. (24) and (25)
	End
6	Obtain samples of $a(t_k)$, $k = 1, 2, \cdots, N_t$
7	Reshape the data and obtain samples of $a(t_k)$ and $a(t_k + 12)$
8	Compute $\hat{\mathbf{P}}(\boldsymbol{\theta})$ using Eqs. (27) and (28) for a given $\boldsymbol{\beta}$ defined in Eq. (17)

The next section discusses how to estimate $\boldsymbol{\theta}$ by solving the optimization model given in Eq. (19).

3.3.2 Estimation of degradation model parameters $\boldsymbol{\theta}$

In this paper, the Generalized Simulated Annealing (GSA) method is used to solve the optimization problem. This method is a stochastic approach for approximating the global optimum of the cost function shown in Eq. (19). The GSA method is mainly used when processing complicated non-linear objective functions with a large number of local minima.

The Cauchy-Lorentz visiting distribution is used to generate a trial jump distance $\Delta\boldsymbol{\theta}(t)$ of the variable $\boldsymbol{\theta}(t)$,

$$\Delta\boldsymbol{\theta}(t) \propto \frac{[T_{q_v}(t)]^{-\frac{D}{3-q_v}}}{[1+(q_v-1)\frac{p^2}{[T_{q_v}(t)]^{\frac{2}{3-q_v}}}]^{\frac{1}{q_v-1}+\frac{D-1}{2}}}, p \sim U(0,1), T_{q_v}(t) = T_{q_v}(1)\frac{2^{q_v-1}-1}{(1+t)^{q_v-1}-1}, \tag{29}$$

where D is the dimension of the variable space, $T_{q_v}(t)$ is the artificial temperature (a time-varying global parameter), and q_v is a time-invariant parameter that controls the rate of cooling. To avoid local minima, the trial jump uses an acceptance probability using a Metropolis algorithm. In other words, the proposed trial jump is always accepted if it is downhill and it is accepted with a probability if the jump is uphill, which allows to explore the space outside the local minima. For more details on this method, the reader is referred to [28,29].

After the parameters $\boldsymbol{\theta}$ are estimated, the degradation model can be used for damage diagnostics and prognostics, which is briefly discussed in the next section.

3.4 Diagnostics and prognostics of using the degradation model

Let $\mathbf{s}_i = [s_{i1}, s_{i2}, \cdots, s_{iN_S}]$ be the strain measurement data at time step t_i, where N_S is the number of strain sensors providing data. The degradation model $a_t = g(t, \boldsymbol{\theta})$ obtained in Sec. 3.3 can then be used for failure diagnostics and prognostics using the approach presented in Vega et al. [16], using the following state and measurement equations,

$$\begin{aligned} &\text{State equation}: a_{k+1} = a_k + \exp(\sigma_{k+1}U_{k+1})Q_{k+1}(a_k)^{w_{k+1}}, \\ &\text{Measurement equation}: \mathbf{s}_{k+1} = \hat{g}(a_{k+1}, \mathbf{x}_{k+1}) + \varepsilon, \end{aligned} \tag{30}$$

where a_{k+1}, a_k, σ_{k+1}, U_{k+1}, Q_{k+1}, and w_{k+1} are, respectively, $a(t_{k+1})$, $a(t_k)$, $\sigma(t_{k+1})$, $U(t_{k+1})$, $Q(t_{k+1})$, and $w(t_{k+1})$ given in Eq. (24). The term $\hat{g}(a_{k+1}, \mathbf{x}_{k+1})$ is a model (e.g., the FE model) for the prediction of strain response for given gap state a_{k+1} and other input variables $\mathbf{x}_{k+1}$ such as water levels and temperature. The measurement noise ε is assumed to be normal, $\varepsilon \sim N(\mathbf{0}, \sigma_{obs}^2 \mathbf{I})$, with uncorrelated structure characterized by the standard deviation σ_{obs}.

Since the original FE model $\hat{g}(a_{k+1}, \mathbf{x}_{k+1})$ is usually expensive, a trained and verified surrogate model, $\hat{g}(a_{k+1}, \mathbf{x}_{k+1})$, is usually used to replace the original FE model. In this paper, a Kriging surrogate modelling method is employed as it can effectively quantify the uncertainty in the prediction, which is advantageous over pointwise-estimate surrogate modelling methods, such as Neural Networks, Support Vector Machine, etc.

The equations above can then be solved recursively in a timely manner as been discussed in Vega et al. [16]. Based on the failure diagnostics and prognostics of the gap growth, the remaining useful life of a miter gate can be estimated at every time step t_k as

$$\Pr\{T_{RUL} \leq t_m \,|\, \mathbf{s}_{1:k}\} = \frac{1}{N_{PF}} \sum_{i=1}^{N_{PF}} \Lambda\{a(i, j+k) > a_e, \exists j = 1, 2, \cdots, m\}, \tag{31}$$

in which T_{RUL} stands for the remaining useful life, N_{PF} is the number of samples used in the state estimation using Eq. (30), a_e is the gap failure threshold, and $a(i, j+k)$ is the i-th realization of the gap length at the $(j+k)$-th time step. In the next section, a miter gate case study is used to demonstrate the effectiveness of the proposed framework.

4 A Case Study

One of the primary concerns of USACE engineers for inspection, maintenance, and repair are the condition of the quoin blocks [3]. Commonly, the deterioration of the quoin blocks is broadly manifested as a small bearing "gap". The formation of this gap is due to the contact degradation between the quoin block attached to the gate and the quoin block attached to the wall that supports the gate laterally. The formation of the bearing gap can be detected using sensor data or from features derived from this data [2,19,30–32]. Figure 6 idealizes the loss of contact in the physical-based FE model and shows the top view of the quoin blocks.

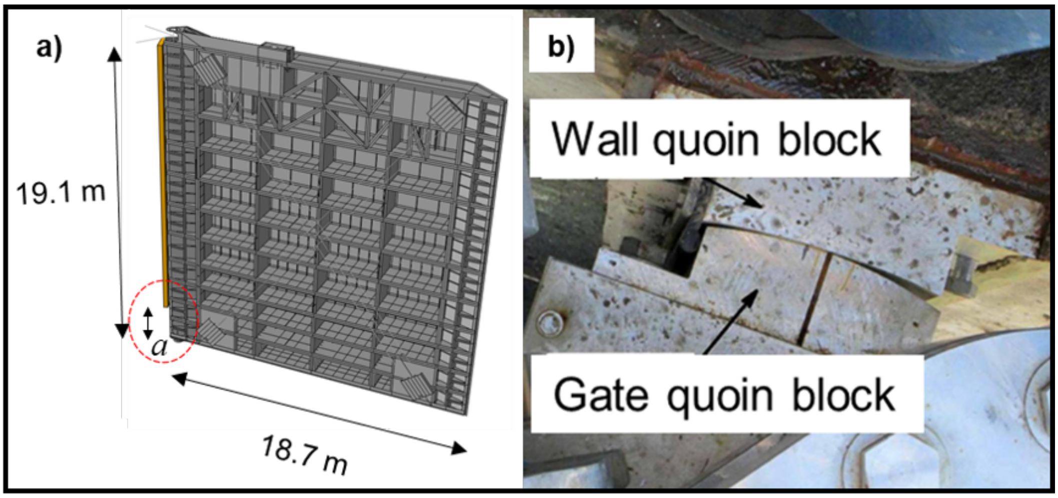

Figure 6: a) Gap formation at the bottom of the quoin blocks and b) the top view of the contact between the quoin blocks [33]

The term $\hat{P}\left(I_{j,t+1}\middle|I_{i,t},\boldsymbol{\theta}\right)$ is the derived transition matrix obtained from the stochastic degradation model. To calculate this matrix, it is necessary to map the gap length value from its continuous form to the discrete OCA ratings using $\boldsymbol{\beta}$ defined in Eq. (17). $\boldsymbol{\beta}$ is also needed in the evaluation of gap length using OCA ratings by the field engineers. Table 2 shows the mapping between gap length, $a(t)$, to its corresponding OCA rating. For the values on this table, the mapping is assumed to be known and would be treated as the inspection policy.

Table 2: Mapping from gap length, $a(t)$, to discrete OCA ratings.

Gap length (cm)	OCA rating
$0 \le a < 76.2$	A
$76.2 \le a < 152.4$	B
$152.4 \le a < 228.6$	C
$228.6 \le a < 304.8$	D
$304.8 \le a < 381$	F
$a > 381$	CF

For the OCA ratings given in the above table, an example of the report OCA transition matrix $\mathbf{P}_{\text{Report}}$ is given as

$$\mathbf{P}_{\text{Report}} = \begin{bmatrix} 7.76e-1 & 2.13e-1 & 5.25e-3 & 2.16e-3 & 1.85e-3 & 2.47e-3 \\ 0 & 9.28e-1 & 4.40e-2 & 1.74e-2 & 7.94e-3 & 2.60e-3 \\ 0 & 0 & 8.70e-1 & 1.19e-3 & 6.64e-3 & 4.78e-3 \\ 0 & 0 & 0 & 9.40e-1 & 5.03e-2 & 9.39e-3 \\ 0 & 0 & 0 & 0 & 8.65e-1 & 1.35e-1 \\ 0 & 0 & 0 & 0 & 0 & 1 \end{bmatrix}. \quad (32)$$

As discussed in Sec. 3, the reported OCA transition matrix may have errors due to the human observation errors of the field engineers. Next, a demonstration is presented of how to obtain the underlying true transition matrix based on the human error matrix using the proposed method. After that, a discussion is presented on how to obtain a gap degradation model and how to use it to perform diagnostics and prognostics.

4.1 Mapping the reported OCA transition matrix to the true OCA transition matrix for different human error scenarios

As indicated by [26], this human error/performance may be evaluated to quantify the reliability or accuracy of these inspections. For demonstration purposes, four different cases as shown in Eqs. (33) to (36) will be evaluated to see the effect of human error on the OCA transition matrix and the degradation model. Case 1 assumes that the inspection is performed without any human observation errors, in other words, $\mathbf{P}_{\text{human}}$ would be the identity matrix. Case 2 represents the behavior of an inspector that regularly tends to assess a structural component to be in a better condition than reality. For example, as shown in Eq. (34), there is a 4% probability that an inspector reports a rating A to a structural component when in reality the true state of the component belongs to rating B. Contrarily, Case 3 represents an inspector that tends to be very conservative. For example, as shown in Eq. (35), there is a 5% probability that an inspector reports a rating F to a structural component when in reality the true state of the component belongs to rating D. Case 4 represents a case in between Case 2 and Case 3.

$$\mathbf{P}_{\text{human}}^{\text{case1}} = \mathbf{I}_{6x6}, \tag{33}$$

$$\mathbf{P}_{\text{human}}^{\text{case2}} = \begin{bmatrix} 1 & 0 & 0 & 0 & 0 & 0 \\ 0.04 & 0.96 & 0 & 0 & 0 & 0 \\ 0 & 0.40 & 0.60 & 0 & 0 & 0 \\ 0 & 0.03 & 0.17 & 0.80 & 0 & 0 \\ 0 & 0 & 0 & 0.03 & 0.97 & 0 \\ 0 & 0 & 0 & 0 & 0.03 & 0.97 \end{bmatrix}, \tag{34}$$

$$\mathbf{P}_{\text{human}}^{\text{case3}} = \begin{bmatrix} 0.60 & 0.40 & 0 & 0 & 0 & 0 \\ 0 & 0.90 & 0.08 & 0.02 & 0 & 0 \\ 0 & 0 & 0.90 & 0.10 & 0 & 0 \\ 0 & 0 & 0 & 0.95 & 0.05 & 0 \\ 0 & 0 & 0 & 0 & 0.98 & 0.02 \\ 0 & 0 & 0 & 0 & 0 & 1 \end{bmatrix}, \tag{35}$$

$$\mathbf{P}_{\text{human}}^{\text{case4}} = \begin{bmatrix} 0.9 & 0.1 & 0 & 0 & 0 & 0 \\ 0.05 & 0.9 & 0.03 & 0.02 & 0 & 0 \\ 0.04 & 0.06 & 0.8 & 0.05 & 0.035 & 0.015 \\ 0.015 & 0.035 & 0.05 & 0.8 & 0.6 & 0.04 \\ 0 & 0.015 & 0.035 & 0.05 & 0.8 & 0.1 \\ 0 & 0 & 0 & 0 & 0 & 1 \end{bmatrix}, \tag{36}$$

As shown in Eq. (10), the true OCA transition matrix ($\mathbf{P}_{\text{OCA}}$) may be obtained after knowing the reported OCA transition matrix ($\mathbf{P}_{\text{Report}}$, Eq. (32)) and the human observation error ($\mathbf{P}_{\text{human}}$, Eqs. (33) through (36)). Using the different cases for human observation errors mentioned earlier, the true OCA transition matrix for each case is shown in Eqs. (37) to (40) respectively.

$$\mathbf{P}_{\mathrm{OCA}}^{\mathrm{case1}} = \begin{bmatrix} 7.76e-1 & 2.13e-1 & 5.25e-3 & 2.16e-3 & 1.85e-3 & 2.47e-3 \\ 0 & 9.28e-1 & 4.40e-2 & 1.74e-2 & 7.94e-3 & 2.60e-3 \\ 0 & 0 & 8.70e-1 & 1.19e-3 & 6.64e-3 & 4.78e-3 \\ 0 & 0 & 0 & 9.40e-1 & 5.03e-2 & 9.39e-3 \\ 0 & 0 & 0 & 0 & 8.65e-1 & 1.35e-1 \\ 0 & 0 & 0 & 0 & 0 & 1 \end{bmatrix}, \quad (37)$$

$$\mathbf{P}_{\mathrm{OCA}}^{\mathrm{case2}} = \begin{bmatrix} 7.02e-1 & 2.89e-1 & 7.01e-3 & 0 & 0 & 2.48e-3 \\ 0 & 9.08e-1 & 7.03e-2 & 1.06e-2 & 8.26e-3 & 2.49e-3 \\ 0 & 0 & 8.42e-1 & 1.47e-1 & 6.04e-3 & 4.73e-3 \\ 0 & 0 & 0 & 9.48e-1 & 4.55e-2 & 6.71e-3 \\ 0 & 0 & 0 & 0 & 8.60e-1 & 1.40e-1 \\ 0 & 0 & 0 & 0 & 0 & 1 \end{bmatrix}, \quad (38)$$

$$\mathbf{P}_{\mathrm{OCA}}^{\mathrm{case3}} = \begin{bmatrix} 7.89e-1 & 2.02e-1 & 3.02e-3 & 1.42e-3 & 1.87e-3 & 2.35e-3 \\ 0 & 9.50e-1 & 2.72e-2 & 1.19e-2 & 8.10e-3 & 2.48e-3 \\ 0 & 0 & 8.40e-1 & 1.48e-1 & 4.27e-3 & 7.46e-3 \\ 0 & 0 & 0 & 8.66e-1 & 1.17e-1 & 1.74e-2 \\ 0 & 0 & 0 & 0 & 8.69e-1 & 1.31e-1 \\ 0 & 0 & 0 & 0 & 0 & 1 \end{bmatrix}, \quad (39)$$

and

$$\mathbf{P}_{\mathrm{OCA}}^{\mathrm{case4}} = \begin{bmatrix} 5.63e-1 & 4.34e-1 & 3.17e-3 & 0 & 0 & 0 \\ 0 & 9.37e-1 & 4.11e-2 & 1.27e-2 & 7.80e-3 & 1.15e-3 \\ 0 & 0 & 8.93e-1 & 9.66e-2 & 8.35e-3 & 1.59e-3 \\ 0 & 0 & 0 & 9.29e-1 & 7.13e-2 & 0 \\ 0 & 0 & 0 & 0 & 9.14e-1 & 8.61e-2 \\ 0 & 0 & 0 & 0 & 0 & 1 \end{bmatrix}, \quad (40)$$

The human observation error has a significant effect on the true OCA transition matrix. For Case 1, the true OCA transition matrix ($\mathbf{P}_{\mathrm{OCA}}^{\mathrm{case1}}$, Eq. (37)) is equal to the reported OCA transition matrix ($\mathbf{P}_{\mathrm{Report}}$, Eq. (32)) and consistent when human observation error is not present. For Case 2, the true OCA transition matrix ($\mathbf{P}_{\mathrm{OCA}}^{\mathrm{case2}}$, Eq. (38)) shows a decrease on the majority of the transition probabilities located in the diagonal when Cases 1 and 2 are compared. In other words, the degradation model should tend to deteriorate faster at the beginning.

Contrarily, the true OCA transition matrix ($\mathbf{P}_{\text{OCA}}^{\text{case3}}$, Eq. (39)) for Case 3 shows that the majority of the transition probabilities located in the diagonal shows an increase when Cases 1 and 3 are compared. Note that not all the diagonal elements show a decrease due to the *error cancellations* in first and second assessments of the OCA ratings. But in general, the degradation model of Case 3 degrades slower than that of Case 1 (as shown in the results in Sec. 4.2). As expected, Case 4 (i.e. Eq. (40)) shows some of the diagonal entries increase while the other diagonals entries decrease when Cases 1 and 4 are compared. Even though effects of the human observation errors on the transition matrix is very complicated due to the "error cancellation" in the OCA ratings, the proposed approach can account for the complicated effects by mapping the reported OCA transition matrix to the true OCA transition matrix.

In the next subsection, the underlying degradation models will be identified based on the obtained OCA transition matrices of different level of human observations errors.

4.2 Gap growth modeling based on OCA transition matrix

Figure 7 shows a flowchart of how to obtain the transition matrix from the stochastic degradation model, which is used to estimate the gap growth model parameters based on the OCA transition matrices obtained above.

Figure 8 shows the cumulative minimum error after each iteration of the stochastic degradation model after tuning 21 parameters for four different cases (i.e. Eq. (33) through (36)). The GSA optimization algorithm successfully achieves a very small error for each case.

Figure 9 presents the simulated gap growth curves corresponding to the four scenarios after identifying the optimal parameters of the gap growth model using GSA. Comparing the gap growth curves of Case 2 to 4 with Case 1, similar conclusions can be obtained as that from comparing the OCA transition matrices (i.e. Eq. (37)-(40)). For Case 2, the degradation model should tend to deteriorate faster at the beginning as shown in Fig. 9, which can also be seen in Fig. 10 when comparing Case 1 and 2. Contrarily, for Case 3, the degradation model should tend to deteriorate slower as shown in Fig. 9, when Cases 1 and 3 are compared.

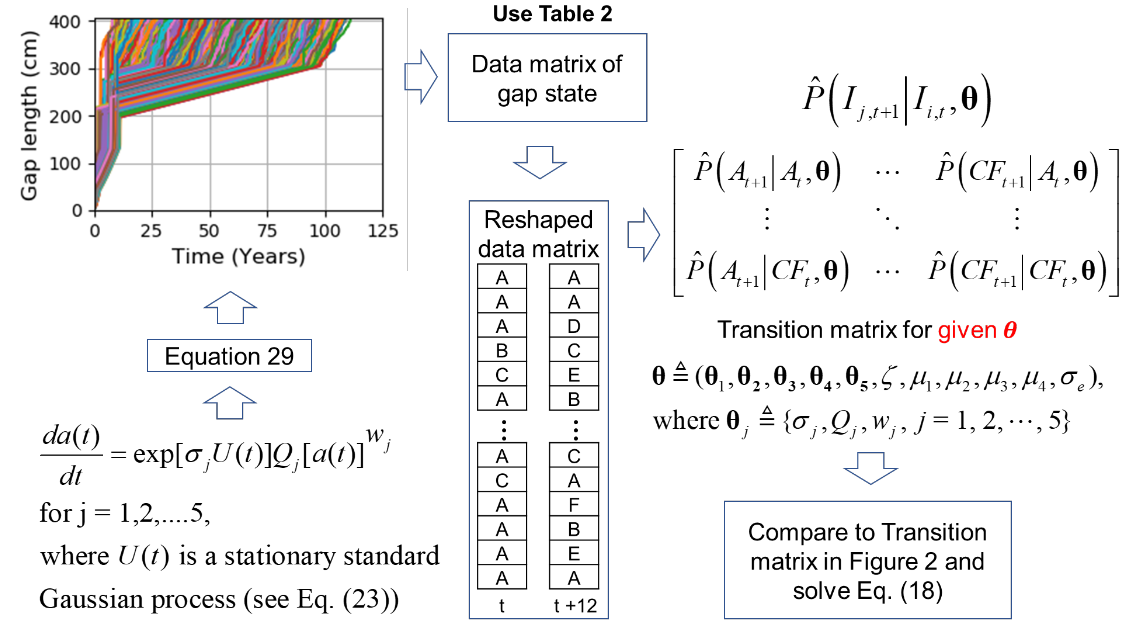

Figure 7: Flowchart to obtain simulated transition matrix from a gap degradation model

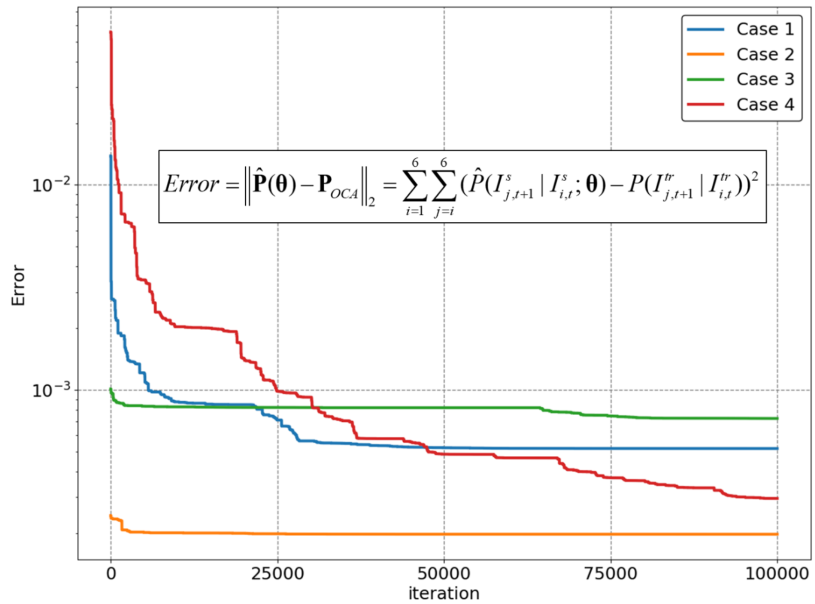

Figure 8: Cumulative minimum error after each iteration

Fig. 10 shows the time distribution when the curves shown in Fig. 9 exceed four different thresholds. As expected, the time distribution for Case 2 shifts to earlier time region (i.e. left) compared to its counterpart of Case 1. Conversely, the time distribution for Case 3 shifts towards later time region (i.e. right) if compared to Case 1. Consistently, the result for Case 4 in general shows time distributions between that of Case 2 and 3.

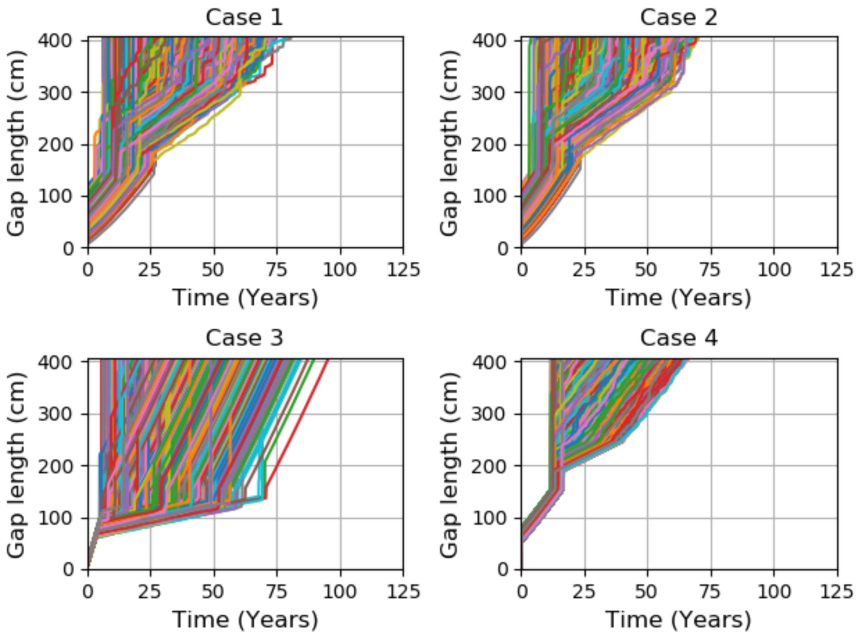

Figure 9: Gap growth model comparison for different human error cases

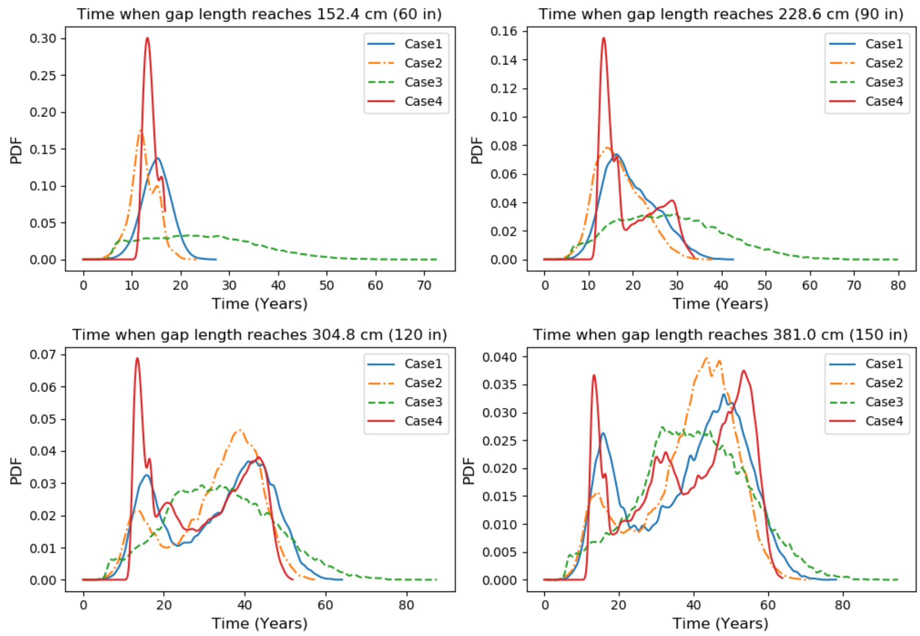

Figure 10: Time distribution when gap length, a, exceeds different damage thresholds for different human error cases

The above results show that the proposed method is able to effectively investigate the effects of human errors on the OCA transition matrix and the gap growth of the gate over time.

4.3 Bearing gap diagnosis and prognosis using SHM and gap growth modeling

Fig. 11 shows the locations where the strain gages are installed based on the SHM strain network installed at the Greenup miter gate (Kentucky, USA). Data is extracted from a FE model of this gate to train a Kriging surrogate model.

Two different surrogate models are built, one that would be used to generate the synthetic data (representing the true physics) and the other to be calibrated during the estimation process. In other words, one surrogate model is built to mimic the reality and the other one to mimic the FE model in the estimation process. Both surrogate models are built from the input and outputs of the FE model after space filling its parameter space. Figure 12(a) shows the updated predictions of the gap length against the true damage using the proposed gap growth model in the estimation process.

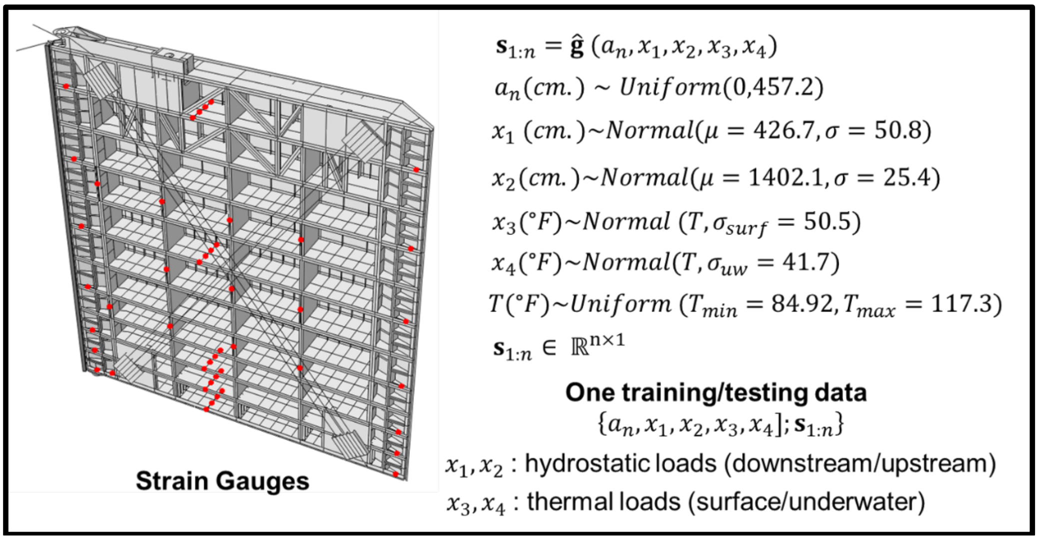

Figure 11: Sensor locations, and data generated to train surrogate model

As shown in Figure 12(b), the proposed method can accurately capture remaining useful life (RUL) while effectively performing damage detection (i.e. Fig. 12 (a)). In addition, the results show that the uncertainty in the RUL estimate can be reduced significantly by mapping the OCA transition matrix into a higher-precision gap growth model, compared to that of the transition matrix-based method as reviewed in Sec. 3. The jumps in Figure 12(b) are attributed to the discrete nature of the OCA ratings, which are more pronounced in the predictions using the TM based approach. More details of the TM approach can be found in [16]. Results of this case study demonstrate the efficacy of the proposed method.

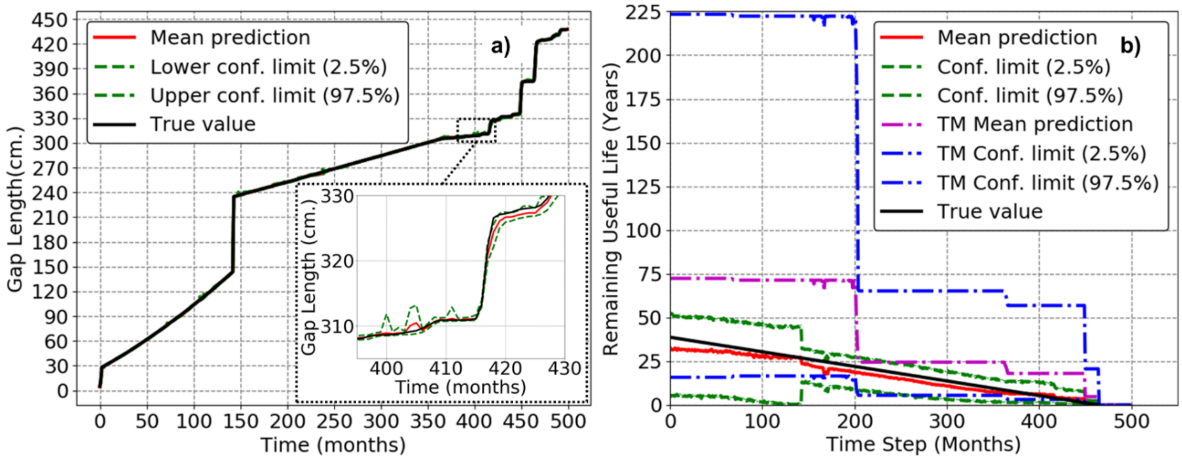

Figure 12: (a) Damage detection over time, and (b) RUL using the proposed method (where "TM" stands for the transition matrix-based approach as reviewed in [16])

5 Discussion

Failure prognostics plays a vital role in proactively scheduling maintenance activities to avoid catastrophic failures, which improves reliability of civil infrastructure and reduce overall life-cycle costs [34–37]. In recent years, data-driven approaches have been developed using neural networks [24,38,39], deep learning [40], and other machine learning-based approaches [41–44] to correlate sensor monitoring data with system degradation and in order to predict system failures. For structures like miter gates, however, historical continuous monitoring data is not available, which makes the state-of-the-art neural network-based approaches inapplicable for failure prognostics of a miter gate. Instead, highly abstracted rating data are available, which contain some kind of degradation information. Along with the highly abstracted data, a high-fidelity physics-based finite element model has been developed to provide some physical understanding of the gate strain response under different conditions. To fully leverage the information of the abstracted ratings and the high-fidelity physics-based simulation model, a new prognostic approach is required. To this end, this paper develops a novel hybrid failure prognostic approach by integrating the highly abstracted OCA ratings with structural health monitoring data.

The developed approach tackles the issue that no viable degradation model available exists for failure prognostics by mapping the corrected OCA transition matrix into a continuous-space degradation model using an optimization-based method. As an optimization-based approach, it is possible that there may be non-unique solutions. To address this issue, the authors plan to develop a fully Bayesian approach to quantify the uncertainty in various model parameters and continuously update the model parameters during the monitoring process methods such as dynamic Bayesian networks. Moreover, more constraints to the optimization model and the OCA transition matrix need to be added in the future to address the potential non-uniqueness issues in the estimation process.

In this paper, a Yang-Manning degradation model is assumed as a potential degradation model. Even though this flexible model allows capturing various gap-growth behavior classes without requiring detailed understanding of the underlying physics, it may not accurately represent the gap degradation pattern in reality. The assumed model may conflict with the subsequent measurement data obtained through an SHM procedure and then affect the inference of the damage states of the system. This is related to the potential model form uncertainty of the assumed degradation model. To address this challenge, the following two research topics are worth investigating in the future: (1) Bayesian model selection and updating using monitoring data to select the best degradation model from multiple candidate models and dynamically updating the model parameters; and (2) dynamic model uncertainty quantification to automatically correct the assumed degradation model during the monitoring process [45].

As mentioned earlier, the framework presented in this work can be applied to other structures with SHM systems installed where very little information about the deterioration rate of a component or system exists, but abstracted inspection data based on ratings are available. For example, this methodology can be used for other structural components of miter gates with different failure modes (e.g., corrosion or pre-tension loss) or even other structures including bridges, pavements and offshore structures due to the availability of inspection ratings performed by several transportation and private agencies.

6 Conclusions

This paper presents a novel hybrid framework for failure diagnostics and prognostics for bearing damaged gaps in the quoin block components of a miter gate. This framework is based on integrating abstracted inspection data and structural health monitoring data, with the following information as inputs:

- Historical visual inspection data given in rating/discrete form;
- Previous knowledge of the human observation errors (i.e., $\mathbf{P}_{human}$);
- A validated physics-based simulation model of the system;
- A known damage threshold to predict the failure;
- Structural health monitoring data (e.g., strain in the present case) at different locations.

This work is especially useful when the evolution of the damage mechanism is not well known or understood either due to the lack of enough data that relates damage to sensor information or the lack of a physics-based model that describes the evolution of the damage. It is assumed that the only available data that describes the damage evolution are based on abstracted rating assessments such as the OCA ratings. An approach is first proposed to map the reported OCA transition matrix into the underlying true OCA transition matrix. Based on that, the proposed framework successfully integrates a stochastic degradation model built from the OCA Markov transition matrix and shows how this model is suitable for integration with continuous monitoring.

The damage diagnosis via physics-based FE model updating using the degradation model proposed provides satisfactory results. Also, to demonstrate the improvement on the gap length prognosis, the updated over time RUL was compared against its true value. Results of a case study show that (1) the proposed framework can effectively address the issue of human reporting errors in the OCA ratings in the prognostics of miter gate, and (2) the uncertainty in the RUL estimate can be reduced significantly using the proposed framework.

Note that, this approach can be applicable to different components in miter gates, which may have different transition matrices values. However, further work needs to be done to extend this methodology from miter gate components to the miter gate system level (e.g. including all critical miter gate components); that work would need to focus on how failure mode probabilities from multiple causes/sources are correlated and propagate towards a more global limit state failure definition. In this paper, optimization-based methods are employed to identify the underlying true OCA transition matrices as well as the gap growth model parameters. These procedures can be integrated together in a full-Bayesian framework. The development of the full-Bayesian framework and the investigation of other alternative approaches will be studied in the future.

Acknowledgements

Funding for this work was provided by the US Army Corps of Engineers through the U.S. Army Engineer Research and Development Center Research Cooperative Agreement W912HZ-17-2-0024.

Appendix A: Derivation of $\Pr\{I_t^{obs}=k, I_{t+1}^{obs}=q\}$

The marginalization of $\Pr\{I_{t+1}^{obs}=q, I_t^{obs}=k\}=\Pr\{I_{t+1}^{obs}=q \mid I_t^{obs}=k\}\Pr\{I_t^{obs}=k\}$ is shown as follows

$$\Pr\{I_{t+1}^{obs}=q, I_t^{obs}=k\} = \sum_{i=1}^{6}\sum_{j=i}^{6}\Pr\{I_{t+1}^{obs}=q, I_t^{obs}=k, I_{t+1}^{tr}=j, I_t^{tr}=i\},$$
$$= \sum_{i=1}^{6}\sum_{j=i}^{6}\Pr\{(I_{t+1}^{obs}=q, I_t^{obs}=k)\,|\,(I_{t+1}^{tr}=j, I_t^{tr}=i)\}\Pr\{I_{t+1}^{tr}=j, I_t^{tr}=i\}. \quad (41)$$

According to the Bayesian network given in Fig. 5, it follows that

$$\Pr\{(I_{t+1}^{obs}=q, I_t^{obs}=k)\,|\,(I_{t+1}^{tr}=j, I_t^{tr}=i)\}$$
$$= \Pr\{I_{t+1}^{obs}=q\,|\,I_{t+1}^{tr}=j, I_t^{obs}=k\}\Pr\{I_t^{obs}=k\,|\,I_t^{tr}=i\}, \quad (42)$$
$$= \frac{\Pr\{I_{t+1}^{obs}=q, I_{t+1}^{tr}=j, I_t^{obs}=k\}}{\sum_{w=k}^{6}\Pr\{I_{t+1}^{obs}=w, I_{t+1}^{tr}=j, I_t^{obs}=k\}}P_{ik}^{h}.$$

Substituting Eq. (42) into Eq. (41) yields

$$\Pr\{I_{t+1}^{obs}=q, I_t^{obs}=k\}$$
$$= \sum_{i=1}^{6}\sum_{j=i}^{6}\left(\frac{\Pr\{I_{t+1}^{obs}=q, I_{t+1}^{tr}=j, I_t^{obs}=k\}}{\sum_{w=k}^{6}\Pr\{I_{t+1}^{obs}=w, I_{t+1}^{tr}=j, I_t^{obs}=k\}}P_{ik}^{h}\right)\Pr\{I_{t+1}^{tr}=j, I_t^{tr}=i\}. \quad (43)$$

The following is obtained from the numerator of Eq. (6)

$$\Pr\{I_{t+1}^{obs}=q, I_{t+1}^{tr}=j, I_t^{obs}=k\} = \Pr\{I_t^{obs}=k\,|\,I_{t+1}^{obs}=q, I_{t+1}^{tr}=j\}P_{jq}^{h}\Pr\{I_{t+1}^{tr}=j\}, \quad (44)$$

where $\Pr\{I_{t+1}^{tr}=j\}$ is solved in Eq. (9). Then, combining Eqs. (43) and (44) yields

$$P_{kq}^{R}\Pr\{I_t^{obs}=k\}$$
$$= \sum_{i=1}^{6}\sum_{j=i}^{6}\left(\frac{\Pr\{I_t^{obs}=k\,|\,I_{t+1}^{obs}=q, I_{t+1}^{tr}=j\}P_{jq}^{h}\Pr\{I_{t+1}^{tr}=j\}}{\sum_{w=k}^{6}\Pr\{I_t^{obs}=k\,|\,I_{t+1}^{obs}=w, I_{t+1}^{tr}=j\}P_{jw}^{h}\Pr\{I_{t+1}^{tr}=j\}}P_{ik}^{h}\right)\Pr\{I_{t+1}^{tr}=j, I_t^{tr}=i\}. \quad (45)$$

Appendix B: A stochastic crack growth model by Yang and Manning [27]

A simple second order approximation for a stochastic crack growth model was proposed by Yang and Manning [27], given by

$$\frac{da(t)}{dt} = X(t)Q(a(t))^{w}, \tag{46}$$

where Q and w are parameters that need to be estimated, and $X(t)$ is modelled as a stationary lognormal stochastic process with a unit mean and an auto-covariance function [27]

$$cov(X(t_1), X(t_2)) = \sigma_x^2 \exp(-\zeta_x |t_2 - t_1|), \tag{47}$$

in which σ_x is the standard deviation of $X(t)$, and ζ_x controls the correlation of $X(t)$ over time. If ζ_x^{-1} approaches to zero, $X(t)$ is a stationary lognormal white noise random process, and the degradation model achieves its most non-conservative stochastic performance. On the other hand, if ζ_x^{-1} approaches infinity, $X(t)$ is a lognormal random variable, and the model becomes the most conservative.

In this paper, a model that is similar to the Yang and Manning model is selected since it does not require a good understanding of the physics and maintains appropriate growth-law features at the same time. The model is given by

$$\frac{da(t)}{dt} = \exp(\sigma_t U(t))Q(a(t))^{w}, \tag{48}$$

in which $\sigma_t > 0$ is a degradation stage-dependent variable and $U(t)$ is a stationary standard Gaussian process with auto-correlation function given by

$$cov(U(t_1), U(t_2)) = \exp(-\zeta |t_2 - t_1|), \tag{49}$$

where ζ is a correlation related parameter similar to Eq. (47). In addition, it is assumed that the degradation model $a_t = g(t, \boldsymbol{\theta})$ consists of N_d distinct degradation stages ($N_d = 5$ in the studied case). Thus, the multi-stage gap growth model is defined as

$$\frac{da(t)}{dt} = \exp(\sigma_i U(t))Q_i(a(t))^{w_i}, i = 1, 2, \cdots, N_d, \tag{50}$$

where $a(t)$ is the gap length at time t, σ_i is a standard deviation variable of degradation stage i, and Q_i and w_i are degradation stage-dependent constants.

Appendix C: Estimation of $\hat{P}(I^s_{j,t+1} \mid I^s_{i,t}; \boldsymbol{\theta}, \mathbf{e})$ based on the simulation of gap growth

As mentioned previously, $\hat{\mathbf{P}}(\boldsymbol{\theta}) \triangleq \{\hat{P}(I^s_{j,t+1} \mid I^s_{i,t}; \boldsymbol{\theta}), i = 1, 2, \cdots, 6; j = i, \cdots, 6\}$, for a given $\mathbf{e} \triangleq \{e_1, e_2, \cdots, e_{N_d - 1}\}$, $\hat{P}(I^s_{j,t+1} \mid I^s_{i,t}; \boldsymbol{\theta}, \mathbf{e})$ is given by

$$\hat{P}(I^s_{j,t+1} \mid I^s_{i,t}; \boldsymbol{\theta}, \mathbf{e}) = \frac{P(I^s_{j,t+1} \cap I^s_{i,t}; \boldsymbol{\theta}, \mathbf{e})}{P(I^s_{i,t}; \boldsymbol{\theta}, \mathbf{e})}, \tag{51}$$

where

$$P(I^s_{i,t}; \boldsymbol{\theta}, \mathbf{e}) = \begin{cases} \Pr\{0 \le a(t) < \beta_i\}, \text{if } i = 1, \\ \Pr\{\beta_{i-1} \le a(t) < \beta_i\}, \text{if } 1 < i < 6, \forall i = 1, 2, \cdots, 6 \\ \Pr\{\beta_{i-1} \le a(t) < \infty\}, \text{if } i = 6, \end{cases} \tag{52}$$

$$\begin{aligned} & P(I^s_{j,t+1} \cap I^s_{i,t}; \boldsymbol{\theta}, \mathbf{e}) = \Pr\{\beta_{i-1} \le a(t) < \beta_i \cap \beta_{j-1} \le a(t+12) < \beta_j\}, \\ & \forall i = 1, 2, \cdots, 6; \; j = i, \cdots, 6, \end{aligned} \tag{53}$$

in which $\beta_0 = 0$, $a(t)$, and $a(t+12)$ are obtained through the degradation model given in Sec. 3.3.1, conditioned on given $\boldsymbol{\theta}$ and $\mathbf{e}$, and $\beta_i = \infty$ or $\beta_j = \infty$ if i=6 or j=6. The two time steps used in Eq. (53) are t and $t+12$ since the inspection interval in the forthcoming case study is one year, and the unit of the time step of the discrete time degradation model (i.e., Eqs. (24) and (25)) is one month.

Since the inspection time t can be any time in the lifetime of the gate, Eqs. (51) through (53) are rewritten as follows

$$\begin{aligned}
&\hat{P}(I^s_{j,t+1} \mid I^s_{i,t}; \boldsymbol{\theta}, \mathbf{e}) \\
&= \int_{t_l}^{t_u} \hat{P}(I^s_{j,t+1} \mid I^s_{i,t}; \boldsymbol{\theta}, \mathbf{e}, t) f(t)\, dt, \\
&= \int_{t_l}^{t_u} \frac{\Pr\{\beta_{i-1} \le a(t) < \beta_i \cap \beta_{j-1} \le a(t+12) < \beta_j\}}{\Pr\{\beta_{i-1} \le a(t) < \beta_i\}} \frac{1}{t_u - t_l} dt,
\end{aligned} \tag{54}$$

where $f(t)$ represents the distribution of the time duration of interest. This distribution is assumed as a uniform distribution bounded by t_l and t_u, which are respectively the lower and upper bounds of the time duration of interest.

In general, Eqs. (54) is analytically intractable due to the complicated transition between stages, even though several analytical expressions have been developed for the degradation model with only one stage based on assumptions and simplifications [27]. In this paper, a simulation-based method is employed. For a given $\boldsymbol{\theta}$ and $\mathbf{e}$, the degradation of the gap is first simulated using the discrete-time model given in Eqs. (24) and (25). From the simulation, the samples obtained of the gap length are denoted as $\mathbf{a}_s(\boldsymbol{\theta}, \mathbf{e}) \triangleq \left\{a_{i,j}, i = 1, 2, \cdots, n_{MCS}; j = 1, 2, \cdots, N_t\right\}$, where $a_{i,j}$ is the i-th realization of the gap growth curve at time step t_j, n_{MCS} is the number of samples at each time step, and N_t is the total number of simulation time steps. Based on the simulated samples of the gap growth, Eq. (54) is approximated as

$$\hat{P}(I^s_{j,t+1} \mid I^s_{i,t}; \boldsymbol{\theta}, \mathbf{e}) \approx \frac{1}{N_t - 12} \sum_{k=1}^{N_t - 12} \frac{\Pr\{\beta_{i-1} \le a(t_k) < \beta_i \cap \beta_{j-1} \le a(t_k + 12) < \beta_j\}}{\Pr\{\beta_{i-1} \le a(t_k) < \beta_i\}}. \tag{55}$$

In the above equation, $\dfrac{\Pr\{\beta_{i-1} \le a(t_k) < \beta_i \cap \beta_{j-1} \le a(t_k + 12) < \beta_j\}}{\Pr\{\beta_{i-1} \le a(t_k) < \beta_i\}}$ is estimated using $\mathbf{a}_s$ as

$$\frac{\Pr\{\beta_{i-1} \le a(t_k) < \beta_i \cap \beta_{j-1} \le a(t_k+12) < \beta_j\}}{\Pr\{\beta_{i-1} \le a(t_k) < \beta_i\}} \approx \frac{1}{n_{MCS}} \frac{\sum_{q=1}^{n_{MCS}} \Lambda((\beta_{i-1} \le a_{q,k} < \beta_i) \cap (\beta_{j-1} \le a_{q,k+12} < \beta_j))}{\sum_{q=1}^{n_{MCS}} \Lambda(\beta_{i-1} \le a_{q,k} < \beta_i)}, \quad (56)$$

where $\Lambda(E)$ is an indicator function such $\Lambda(E)=1$ if event E is true and $\Lambda(E)=0$ if event E is false. In the above equation, event E represents $(\beta_{i-1} \le a_{q,k} < \beta_i) \cap (\beta_{j-1} \le a_{q,k+12} < \beta_j)$ and $\beta_i \le a_{q,k} < \beta_{i+1}$.

References

[1] U.S. Army Corps of Engineers Headquarters. Navigation 2018. http://www.usace.army.mil/Missions/CivilWorks/Navigation.aspx (accessed August 1, 2018).

[2] Eick BA, Treece ZR, Spencer BF, Smith MD, Sweeney SC, Alexander QG, et al. Automated damage detection in miter gates of navigation locks. Struct Control Heal Monit 2018;25:1–18. https://doi.org/10.1002/stc.2053.

[3] Foltz SD. Investigation of Mechanical Breakdowns Leading to Lock Closures. Champaign, IL: 2017.

[4] Przybyla J. Best Practices in Asset Management. Alexandria, Virginia: 2013.

[5] USACE. Policy for Operational Condition Assessments of USACE Assets 2019:13. https://www.publications.usace.army.mil/Portals/76/Users/182/86/2486/EC-11-2-218.pdf?ver=2019-09-04-162858-440.

[6] U.S. Army Corps of Engineers Headquarters. SMART GATE 2007. https://www.erdc.usace.army.mil/Media/Fact-Sheets/Fact-Sheet-Article-View/Article/476668/smart-gate/ (accessed August 1, 2018).

[7] Graybeal BA, Phares BM, Rolander DD, Moore M, Washer G. Visual inspection of highway bridges. J Nondestruct Eval 2002;21:67–83. https://doi.org/10.1023/A:1022508121821.

[8] Orcesi AD, Cremona CF. A bridge network maintenance framework for Pareto optimization of stakeholders/users costs. Reliab Eng Syst Saf 2010;95:1230–43. https://doi.org/10.1016/j.ress.2010.06.013.

[9] Calvert G, Neves L, Andrews J, Hamer M. Multi-defect modelling of bridge deterioration using truncated inspection records. Reliab Eng Syst Saf 2020;200. https://doi.org/10.1016/j.ress.2020.106962.

[10] Zhang X, Gao H. Road maintenance optimization through a discrete-time semi-Markov decision process. Reliab Eng Syst Saf 2012;103:110–9. https://doi.org/10.1016/j.ress.2012.03.011.

[11] Abaza KA. Empirical approach for estimating the pavement transition probabilities used in non-homogenous Markov chains. Int J Pavement Eng 2017;18:128–37. https://doi.org/10.1080/10298436.2015.1039006.

[12] Zhang Y, Kim C-W, Tee KF. Maintenance management of offshore structures using Markov process model with random transition probabilities. Struct Infrastruct Eng 2017;13:1068–80. https://doi.org/10.1080/15732479.2016.1236393.

[13] Mohseni H, Setunge S, Zhang G, Wakefield R. Markov Process for Deterioration Modeling and

Asset Management of Community Buildings. J Constr Eng Manag 2017;143:04017003. https://doi.org/10.1061/(ASCE)CO.1943-7862.0001272.

[14] Niu G, Yang B-S, Pecht M. Development of an optimized condition-based maintenance system by data fusion and reliability-centered maintenance. Reliab Eng Syst Saf 2010;95:786–96. https://doi.org/10.1016/j.ress.2010.02.016.

[15] Wang C, Elsayed EA. Stochastic modeling of corrosion growth. Reliab Eng Syst Saf 2020;204:107120. https://doi.org/10.1016/j.ress.2020.107120.

[16] Vega MA, Hu Z, Todd MD. Optimal maintenance decisions for deteriorating quoin blocks in miter gates subject to uncertainty in the condition rating protocol. Reliab Eng Syst Saf 2020;204. https://doi.org/10.1016/j.ress.2020.107147.

[17] Alaswad S, Xiang Y. A review on condition-based maintenance optimization models for stochastically deteriorating system. Reliab Eng Syst Saf 2017;157:54–63. https://doi.org/10.1016/j.ress.2016.08.009.

[18] Baraldi P, Mangili F, Zio E. Investigation of uncertainty treatment capability of model-based and data-driven prognostic methods using simulated data. Reliab Eng Syst Saf 2013;112:94–108. https://doi.org/10.1016/j.ress.2012.12.004.

[19] Vega MA, Ramancha MR, Conte JP, Todd MD. Efficient Bayesian Inference of Miter Gates using High-Fidelity Models. 38th Int. Modal Anal. Conf., Houston, Texas: Springer; 2021.

[20] Ramancha MK, Astroza R, Conte JP, Restrepo JI, Todd MD. Bayesian Nonlinear Finite Element Model Updating of a Full-Scale Bridge-Column using Sequential Monte Carlo. 38th Int. Modal Anal. Conf., Houston, Texas: Springer; 2020.

[21] Yang Y, Madarshahian R, Todd MD. Bayesian Damage Identification Using Strain Data from Lock Gates, Springer,; 2019, p. 47–54. https://doi.org/10.1007/978-3-030-12115-0_7.

[22] Gomez F, Spencer, Jr. BF, Smith MD. Bayesian Modeling Updating of Miter Gates with Uncertain Boundary Conditions. Struct. Heal. Monit. 2019, Lancaster, PA: DEStech Publications, Inc.; 2019. https://doi.org/10.12783/shm2019/32129.

[23] Smith M, Fillmore T. Methodology supporting Civil Works implementation of tainter gate trunnion friction structural health monitoring. 2018. https://doi.org/10.21079/11681/29975.

[24] Vega MA, Todd MD. A variational Bayesian neural network for structural health monitoring and cost-informed decision-making in miter gates. Struct Heal Monit 2020. https://doi.org/10.1177/1475921720904543.

[25] Vega MA, Madarshahian R, Fillmore TB, Todd MD. Optimal Maintenance Decision for Deteriorating Components in Miter Gates Using Markov Chain Prediction Model. Struct. Heal. Monit. 2019 Enabling Intell. Life-cycle Heal. Manag. Ind. Internet Things, Lancaster, PA: DEStech Publications, Inc.; 2019, p. 1471–8. https://doi.org/10.12783/shm2019/32269.

[26] Campbell LE, Connor RJ, Whitehead JM, Washer GA. Benchmark for Evaluating Performance in Visual Inspection of Fatigue Cracking in Steel Bridges. J Bridg Eng 2020;25:04019128. https://doi.org/10.1061/(ASCE)BE.1943-5592.0001507.

[27] Yang JN, Manning SD. A simple second order approximation for stochastic crack growth analysis. Eng Fract Mech 1996;53:677–86. https://doi.org/10.1016/0013-7944(95)00130-1.

[28] Xiang Y, Gubian S, Suomela B, Hoeng J. Generalized Simulated Annealing for Global Optimization: The GenSA Package. R J 2013;5:13. https://doi.org/10.32614/RJ-2013-002.

[29] Xiang Y, Gong XG. Efficiency of generalized simulated annealing. Phys Rev E 2000;62:4473–6. https://doi.org/10.1103/PhysRevE.62.4473.

[30] Hoskere V, Eick B, Spencer BF, Smith MD, Foltz SD. Deep Bayesian neural networks for damage quantification in miter gates of navigation locks. Struct Heal Monit 2019:147592171988208. https://doi.org/10.1177/1475921719882086.

[31] Eick BA, Treece, Zachary R., Spencer Jr. BF, Smith MD, Sweeney SC, Alexander QG, Foltz SD. Miter Gate Gap Detection Using Principal Component Analysis. 2017.

[32] Vega M, Madarshahian R, Todd MD. A Neural Network Surrogate Model for Structural Health Monitoring of Miter Gates in Navigation Locks. 37th Int. Modal Anal. Conf., Orlando, Florida: 2019, p. 93–8. https://doi.org/10.1007/978-3-030-12075-7_9.

[33] Daniel R, Paulus T. Hydraulic Gates in View of Asset Management. Lock Gates Other Closures Hydraul. Proj., Elsevier; 2019, p. 945–60. https://doi.org/10.1016/B978-0-12-809264-4.00017-3.

[34] Zhao Y. On preventive maintenance policy of a critical reliability level for system subject to degradation. Reliab Eng Syst Saf 2003;79:301–8. https://doi.org/10.1016/S0951-8320(02)00201-6.

[35] van Noortwijk JM, Frangopol DM. Deterioration and Maintenance Models for Insuring Safety of Civil Infrastructures at Lowest Life-Cycle Cost. Life-Cycle Perform. Deterior. Struct., Reston, VA: American Society of Civil Engineers; 2003, p. 384–91. https://doi.org/10.1061/40707(240)39.

[36] Le Son K, Fouladirad M, Barros A, Levrat E, Iung B. Remaining useful life estimation based on stochastic deterioration models: A comparative study. Reliab Eng Syst Saf 2013;112:165–75. https://doi.org/10.1016/j.ress.2012.11.022.

[37] Li R, Arzaghi E, Abbassi R, Chen D, Li C, Li H, et al. Dynamic maintenance planning of a hydro-turbine in operational life cycle. Reliab Eng Syst Saf 2020;204:107129. https://doi.org/10.1016/j.ress.2020.107129.

[38] Zhang X, Xiao L, Kang J. Degradation Prediction Model Based on a Neural Network with Dynamic Windows. Sensors 2015;15:6996–7015. https://doi.org/10.3390/s150306996.

[39] Khan F, Eker O, Khan A, Orfali W. Adaptive Degradation Prognostic Reasoning by Particle Filter with a Neural Network Degradation Model for Turbofan Jet Engine. Data 2018;3:49. https://doi.org/10.3390/data3040049.

[40] Zhang L, Gao H, Wen J, Li S, Liu Q. A deep learning-based recognition method for degradation monitoring of ball screw with multi-sensor data fusion. Microelectron Reliab 2017;75:215–22. https://doi.org/10.1016/j.microrel.2017.03.038.

[41] Zio E, Di Maio F. A data-driven fuzzy approach for predicting the remaining useful life in dynamic failure scenarios of a nuclear system. Reliab Eng Syst Saf 2010;95:49–57. https://doi.org/10.1016/j.ress.2009.08.001.

[42] Mohanty S, Das S, Chattopadhyay A, Peralta P. Gaussian Process Time Series Model for Life Prognosis of Metallic Structures. J Intell Mater Syst Struct 2009;20:887–96. https://doi.org/10.1177/1045389X08099602.

[43] Galar D, Kumar U, Lee J, Zhao W. Remaining Useful Life Estimation using Time Trajectory Tracking and Support Vector Machines. J Phys Conf Ser 2012;364:012063. https://doi.org/10.1088/1742-6596/364/1/012063.

[44] Ye Z-S, Xie M. Stochastic modelling and analysis of degradation for highly reliable products. Appl Stoch Model Bus Ind 2015;31:16–32. https://doi.org/10.1002/asmb.2063.

[45] Hu Z, Hu C, Mourelatos ZP, Mahadevan S. Model Discrepancy Quantification in Simulation-Based Design of Dynamical Systems. J Mech Des 2019;141:1–13. https://doi.org/10.1115/1.4041483.